Aalto University
School of Engineering
Civil Engineering Department

Chemical analysis and microstructure of concrete after long-term exposure to LILW repositories condition – Part II

PERCO2 / WP1 – Durability testing of existing concrete specimens

Fahim Al-Neshawy and Abobaker Ba Ragaa

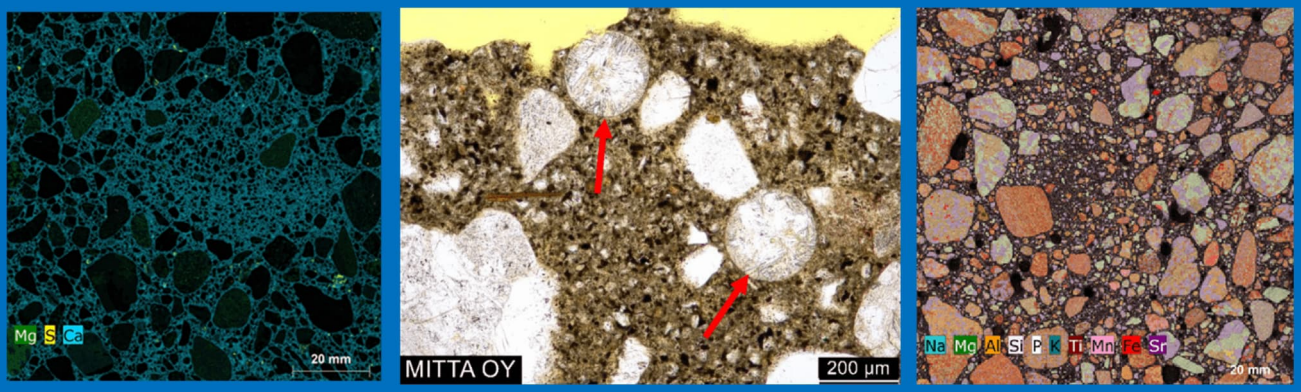

Aalto University School of Engineering, Department of Civil Engineering
PL 12100, FI-00076 AALTO
http://civileng.aalto.fi

Table of Contents

1. Introduction

1.1 Long-term durability testing – history of the investigation

In 1997 a joint project of Teollisuuden Voima Oyj (TVO) and Fortum Power and Heat oy was started for acquisition of real testing data on the performance of concrete barriers in final disposal conditions. A comprehensive set of concrete specimens was made with different type of binders using different water-binder ratios. The test specimens were placed in water solutions which simulate the chemical composition of ground water. The samples were first stored in a parking garage in Myyrmäki but were removed in the shift of the year 2010 - 2011 to the VLJ-depository in Olkiluoto. The analysis of the microstructures and chemical analysis of the concrete were investigated at different age of the concrete specimens to assess their condition:

1) 1999 – Ipatti, A., Betonin pitkäaikaissäilyvyys loppusijoitusolosuhteissa, Koebetonien lähtö tilanneanalyysien vertailua. Fortum Teknologia, Muistio TECH- 1441; 4.1 1.1999, 4s + 2 liitesivua.
   In the research, test program for determining the long-term durability of concrete was initiated. In the research report, the initial levels of sulphate (S), Magnesium (Mg), and Chloride (Cl) concentrations in the test concretes were obtained from the test concretes by the end of the project year 1999.
2) 2012 – Vesikari, E. and Koskinen, P. “Durability of Concrete Barriers in Final Depositories of Nuclear Waste,” Espoo, Feb. 2012 [1].
   In this research, analysing of concrete samples which have been 13 years immersed in water solutions were performed. The research project was a part of the Finnish research programme on nuclear waste management “KYT 2014”. The final aim of the research was to elevate the level of knowledge on the durability of concrete barriers in final disposal conditions, i.e. below the ground water, and to acquire data for modelling the performance of concrete over time. Based on these results the aim is to develop methodologies for evaluating the service life of such barriers.
3) 2023 – Ba Ragaa, A. (2023). Long-term durability testing of concrete in low and intermediate level waste repositories [2].
   In this study, the aim was to evaluate the durability of concrete mixes that can be used in LILW repositories. The study was conducted by examining concrete specimens made with different binders and stored for ~25 years in different storage solutions that simulate the environment in LILW repositories.

1.1 Durability of concrete exposed to sulphate attacks

Sulphate attack is the term used to describe a series of chemical reactions between sulphate ions and the components of hardened concrete, principally the cement paste, caused by exposure of concrete to sulphates and moisture. It is usually known as a process of deterioration that targets concrete durability by expansion, degradation and decomposition of hydrated cement paste.

In this mechanism of deterioration, sulphate ions, depending on their cation type, take part in different chemical reactions with hydrated compounds inside cement paste and result in

formation of different compounds such as gypsum, monosulfoaluminate (also called monosulphate), ettringite, and thaumasite. Sulphate solutions containing Ca, Na, Mg, and Fe as the cation are the most usual types in sulphate attack.

With respect to the source of ions, sulphate attack can be characterized as:

1) internal sulphate attack (ISA) that occurs when sulphates are present inside concrete during manufacture. Cement, supplementary cementing materials, aggregates, chemical admixtures, and water are different possible sources of sulphate ions for internal sulphate attack.
2) external sulphate attack (ESA) is the most common one. In this process, sulphate solutions from various sources such as ground water, soil, solid and liquid industrial wastes, fertilizers, and atmospheric SO_3 penetrate into hydrated cement paste and start reactions associated with sulphate attack [3].

Ettringite sulphate attack is the most common mechanism of sulphate deterioration in which sulphate bearing solutions react with the hydrated cement matrix. Generally, the result of this type of deterioration is formation of gypsum and ettringite. The typical reactions associated with formation of gypsum and ettringite are presented in Equation (1) and Equation (2).

$$Ca(OH)_2 + SO_4^{2-} + 2H_2O \rightarrow CaSO_4 \cdot 2H_2O\ (gypsum) + 2OH^-$$
$$3CaO \cdot Al_2O_3 + (CaSO_4 \cdot 2H_2O) + 26H_2O \rightarrow 3CaO \cdot Al_2O_3 \cdot 3CaSO_4 \cdot 32H_2O \quad (1)$$
$$tricalcium\ aluminate + gypsum + water \rightarrow ettringite$$

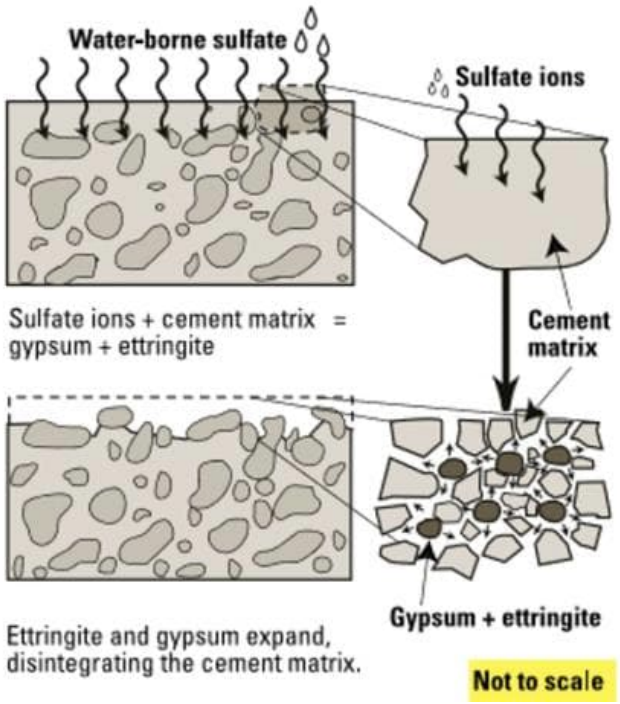

Figure 1. Illustration of the external sulphate attack [4].

Basically, sulphate ions react with calcium hydroxide and form gypsum. Following that reaction, gypsum itself reacts with calcium aluminate hydrates inside the hydrated cement paste and results in formation of ettringite. Both gypsum and ettringite are larger in volume than the reactants in this process; therefore, their formation is expansive. When the concentration of sulphate ions decreases, ettringite breaks down into monosulphate aluminates (AFm):

$$\begin{aligned} 2CaO \cdot Al_2O_3 + 3CaO \cdot Al_2O_3 \cdot 3CaSO_4 \cdot 32H_2O \\ \rightarrow 3CaO \cdot Al_2O_3 \cdot 3CaSO_4 \cdot 12H_2O \end{aligned} \quad (2)$$

$$\begin{aligned} Tricalcium\ aluminate\ +\ ettringite \\ \rightarrow\ monosulfate\ aluminates\ (AFm) \end{aligned}$$

The main problem with ordinary sulphate attack lies in expansion, cracks and deformation inside the hydrated cement paste that might cause serious problems in structural concrete. Evidently, formation of cracks during this process increases the pace of deterioration by increasing concrete permeability and facilitating a more sulphate bearing solution to penetrate into concrete. Examples of formation of ettringite in hydrated cement paste are shown in Figure 2.

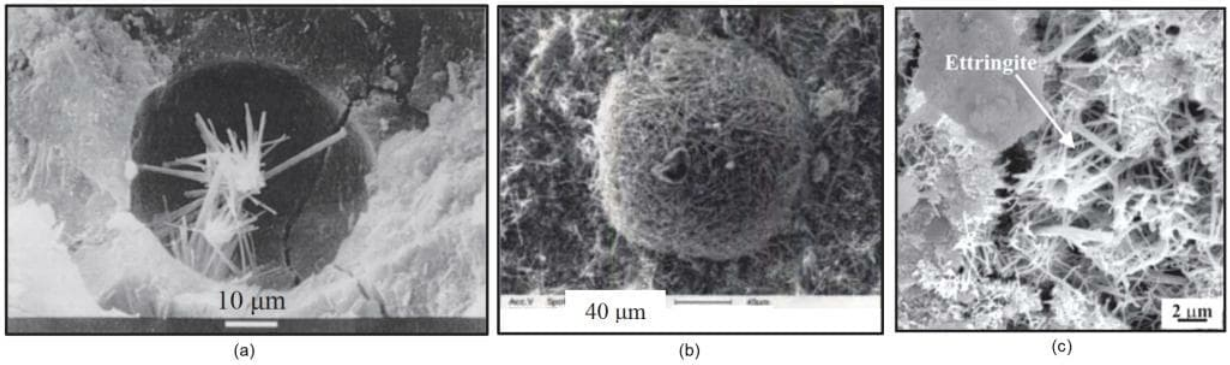

Figure 2. (a) Scanning Electron Microscopy (SEM) image depicting a crack and ettringite needles on the fractured surface of a mortar sample, (b) Entrained air bubble filled with needles of ettringite and (c) ettringite crystals in cement paste [3].

Leaching is a diffusion-reaction phenomenon which takes place when concrete is exposed to poorly mineralized or acid water. Degradation consists in dissolution of calcium and hydroxide ions out of the matrix, which causes an increase in porosity and transport properties of surface concrete [5]. Leaching is accelerated in neutral and acid solutions, and it may be coupled with the ingress of aggressive ions such as chloride, sulphate, magnesium [6]. These issues need to be taken into consideration in the design of concrete structures in contact with ground water–such as nuclear waste containers and also nuclear cooling towers, wastewater treatment plants and precast concrete products such as water tanks and sewage pipes [7].

1.2 Degradation of concrete under coupled chloride and sulphate attack

In some salt-alkali regions, where the environment contains high concentrations of sulphates and chlorides, reinforced concrete will be attacked by both chloride and sulphate

ions. Concrete structures long exposed to these salt-alkali environments and coastal salt soils present corrosion evidence due to chloride ions as well as sulphate ions, resulting in decreased durability and shortened service life[8], [9]. The corrosion mechanisms of reinforced concrete structures are quite complex when chloride and sulphate ions coexist. A study of the degradation mechanisms of reinforced concrete under chloride and sulphate coupling is therefore of great importance to assess durability and predict the service life of concrete structures in marine environments and elsewhere, as well as to examine the mutual influence of the coupled processes on concrete deterioration and steel corrosion.

The degradation mechanisms of the decoupled phenomena of chloride and sulphate attack on cementitious materials are quite clear. Because chloride and sulphate ions interact, concrete deteriorates differently under a combined diffusion of chloride and sulphate than under each damage factor individually. This results in strongly coupled effects.

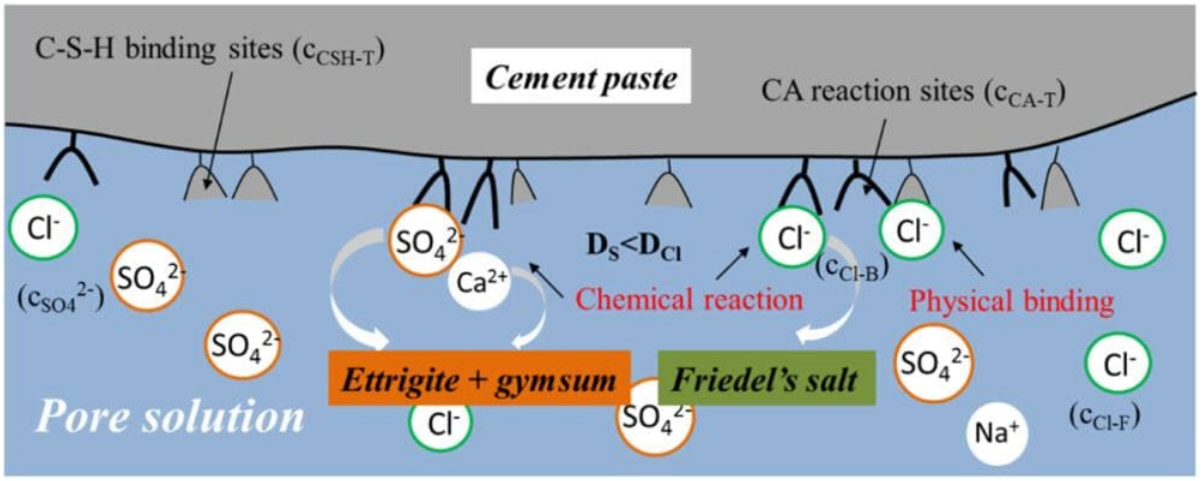

Figure 3. Schematic diagram of the interaction between penetrated ions and hardened cement pastes [10].

Chlorides and sulphates penetrate into concrete by means of capillary suction and diffusion, so diffusivity is the transport mechanism determining penetration and attack of ions. At early stage, the accumulation of reaction products (i.e. gypsum, ettringite and Friedel's salt, etc) could decrease the available pore volume of concrete and thereby inhibits the transport of ions into the concrete.

The increase of ettringite formation gradually accelerates the expansion of concrete with time, ultimately leading to a more serious cracking and chloride-induced corrosion of reinforcement bars in concrete. Furthermore, there is a competitive binding between chlorides and sulphate ions with the calcium aluminate (CA) binding sites (i.e. hydrated and unhydrated calcium aluminate). It was found that chloride ions penetrate into concrete and react with monosulfoaluminate to form Friedel's salt, which could release sulphate ions by reducing the formation of ettringite, as presented in Figure 3. Due to the combination of chloride ions by aluminate phases in concrete, more sulphate ions is able to transport into the concrete further. The competitive relation between chloride and sulphate ions is also influenced by temperature and calcium ion (Ca^{2+}), which facilitated the stabilized the C-S-H phase [10].

2. Characteristics of concrete and storage conditions

2.1 Cementitious materials and binders

The test on concrete specimens was designed to assess chemical resistance of cements or binders of concrete exposed to sodium sulphate and chloride attacks for 27 years (1997 – 2024). Three types of binders for the test series started in 1997 by TVO and Fortum power companies produced by the Finnsementti Oy [11] were used, namely:

- Sulphate resisting cement CEM I 42.5
- General (Yleis) Portland cement CEM II 42.5 R + 10% Micropoz Silica Fume
- (Mega) Portland cement CEM I 42.5 R + 10% KJ-400 Ground Granulated Blast-furnace Slag (GGBS) + 5% Micropoz Silica Fume.

The compositions of the binders are presented in Table 1.

Table 1: Binder types used for testing.

Binder code	Cement	Ground Granulated Blast-furnace Slag.(GGBS)	Silica fume
S1	SR cement (CEM I 42.5 SR)100%	0%	0%
S2	"Yleis"cement (CEM II A 42.5 R) 90%	0%	10%
S3	"Mega" cement (CEM I 42.5 R) 20%	75%	5%

2.2 Concrete mixtures

Three concrete mixtures were selected for this research using three different cementitious materials (Table 1). The selected concrete mixtures have the same water to binder ratio of 0,425 and aggregate to binder ration of 5,0. The mix design of concrete adapted from the Ipatti (2010) report [12], is presented in Table 2.

Table 2. Concrete mix design.

	B2	B5	B8
Binder type (see Table 1)	S1	S2	S2
Cement content (kg/m³)	373	337	74
KJ-400 GGBS slag content (kg/m³)	–	–	279
Micropoz Silica Fume content (kg/m³)	–	37	19
Aggregate content (kg/m³)	1867	1857	1862
Water content + Superplasticizer (dm³)	159	158	158
Superplasticizer (% wt. of binder)	0,80	3,30	1,10
Total content (kg/m³)	2400	2386	2391

Figure 4. Selected concrete specimens for the investigation.

2.3 Properties of concrete

The target slump for the concrete mix was set at 120 - 140 mm. The consistency of the test concretes was adjusted to the target value using a naphthalene sulfonate-based Fliessmittel SF superplasticizer. The following fresh concrete properties were determined for the test concretes. Slump ofocrete (SFS 5284), density (SFS 5288), and air content (SFS 5287) were measured 10, 40, and 70 minutes after the concrete was mixed. The results of the fresh concrete tests are presented in Table 3.

Table 3. Properties of fresh concrete.

		B2	B5	B8
Casting date / 1998		19.01	29.01	09.02
Slump (mm)	10 min	120	125	115
	40 min	65	100	80
	70 min	35	80	50
Density (kg/m³)	10 min	2420	2410	2400
	40 min	2430	2400	2400
	70 min	2430	2400	2400
Air content, (%)	10 min	2,6%	2,4%	2,1%
	40 min	2,2%	2,3%	2,2%
	70 min	2,2%	2,3%	2,1%

Compressive strength (SFS 4474) concrete specimens were tested at the ages of 7, 28, 91, and 182 days, as well as at 1, 2, 3, 5, 8, 12.5, and 15 years, with three 150 mm cubes per test concrete were tested at each testing age. The molds were removed at 1 day of age, after which the test specimens were stored in water.

Modulus of elasticity (SFS 5450) concrete specimens were tested at 91 days, as well as at 1, 2, 3, 5, 8, 12.5, and 15 years of age. Two cylinders per test concrete were

tested at each testing age. The molds were removed at 1 day of age, after which the test specimens were stored in water at +12 ± 1°C.

Table 4. Properties of hardened concrete.

		B2	B5	B8
Casting date / 1998		19.01	29.01	09.02
Compressive strength (MPa)	7d	47,5	47,0	14,5
	28d	58,5	63,0	38,5
	91d	66,0	74,5	54,0
	182d	73,0	77,5	60,0
	1 year	77,0	83,5	64,5
	2 years	69,0	76,0	57,0
	3 years	81,0	87,0	68,5
	5 years	83,0	87,5	67,5
	8 years	84,5	89,5	71,0
	12.5 years	84,0	90,0	70,0
Modulus of elasticity (GPa	91d	34.6	33.6	33.6
	1 year	34.1	34.6	34.5
	2 years	35.8	34.8	34.8
	3 years	36.0	36.2	36.4
	5 years	36.3	36.6	39.0
	8 years	41.3	39.9	40.6
	12.5 years	40.0	39.7	40.5

2.4 Storage conditions

The specimens tested in this research report were stored in three different salt solutions. The salt solutions were prepared aiming to simulate the sulphate, chloride and magnesium ions concentration of the ground water at Olkiluoto ja Loviisa. The solutions are presented in Table 5.

Table 5: The used water solution and their aggressive component content.

Solution code	Chemical	Aggressive ions	Ion concentration (mg/dm³)
L7	Na_2SO_4 +NaCl + $MgCl.6H_2O$	SO_4	20
		Cl	50
		Mg	50
L8	Na_2SO_4 +NaCl + $MgCl.6H_2O$	SO_4	500
		Cl	1000
		Mg	100
GW (Olkiluoto – Groundwater)		SO_4	45
		Cl	17
		Mg	0,16

3. Experimental procedures

Chemical analysis of the concrete specimens was performed using the micro-X-ray fluorescence method and the chloride titration method. The petrographic analysis of the concrete specimens was used for analysing the microstructure of concrete.

3.1 Micro X-ray Fluorescence (µXRF)

Fluorescence is based on the property of some molecules that when they are hit by a photon, they can absorb the energy of that photon to get into an excited state. Upon relaxation from that excited state, the same molecule releases a photon: fluorescence emission.

A regular pigment can absorb visible light (what we call “white” light which is a combination of all wavelengths the human eye can detect), and then reflect some light in the same part of the spectrum. For example, a green pigment can absorb white light, but the pigment will reflect the “green” wavelengths allowing the eye to perceive the color green.

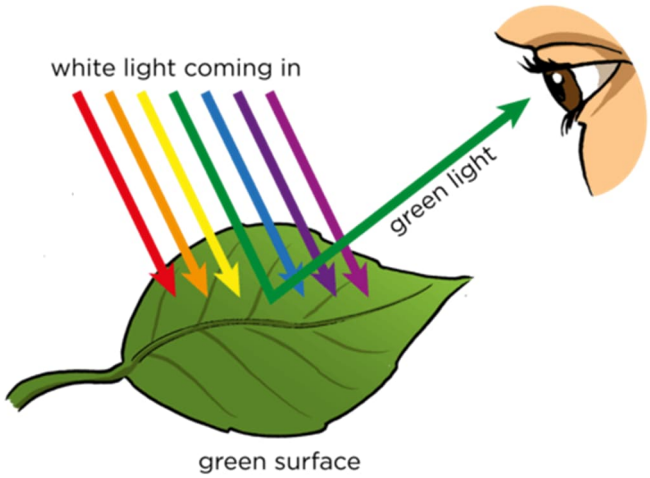

Figure 5. Principle of fluorescence.

XRF is based on the principle that each element has a unique atomic structure and emits a specific wavelength of X-ray radiation when it is excited by a high-energy source. *By detecting and analyzing the intensity and energy of the emitted X-rays, XRF can identify and quantify the elements in the sample.* XRF (X-ray fluorescence) is a non-destructive analytical technique used to determine the elemental composition of materials. XRF analyzers determine the chemistry of a sample by measuring the fluorescent (or secondary) X-ray emitted (radiated) from a sample when it is excited by a primary X-ray source. Each of the elements present in a sample produces a set of characteristic fluorescent X-rays (“a fingerprint”) that is unique for that specific element, which is why XRF spectroscopy is an excellent technology for qualitative and quantitative analysis of material composition [13].

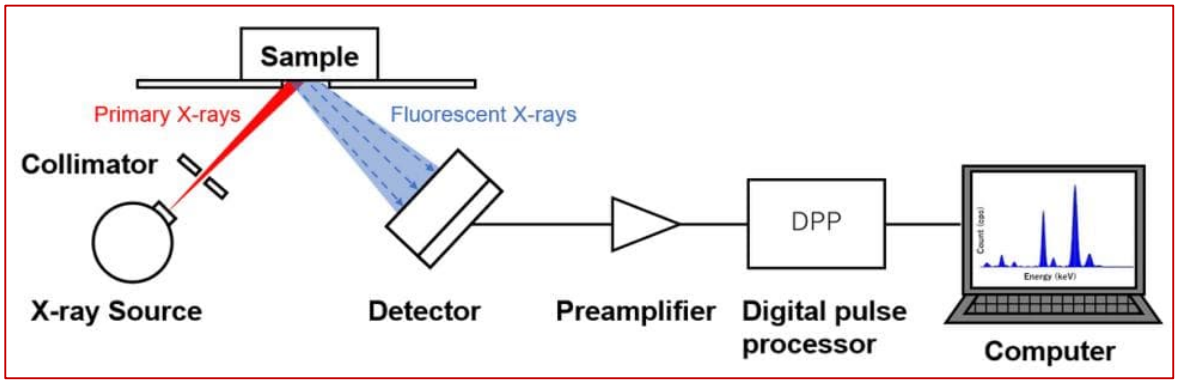

Figure 6. Key Components of X-ray Fluorescence (XRF) Spectrometer.

Micro X-ray fluorescence (µXRF) is an elemental analysis technique which allows for the examination of very small sample areas. Like conventional XRF instrumentation, Micro X-ray Fluorescence uses direct X-ray excitation to induce characteristic X-ray fluorescence emission from the sample for elemental analysis. Unlike conventional XRF, which has a typical spatial resolution ranging in diameter from several hundred micrometres up to several millimetres, µXRF uses X-ray optics to restrict the excitation beam size or focus the excitation beam to a small spot on the sample surface so that small features on the sample can be analysed.

X-ray energy forms the basis for insightful measurement techniques. Energy dispersive X-ray fluorescence identifies metals and elements in an object by detecting their signature XRF emission energies. Essentially, all elements have a fixed number of electrons arranged in atomic orbitals around their nuclei. When photons from the X-ray tube strike the object of interest with enough energy to expel the electrons out of the elements' innermost orbitals, the atoms become unstable.

To regain stability, electrons from the outer orbitals move into the newly vacant spaces in the inner orbitals. As an electron transitions from an outer orbital to an inner orbital, it emits photon energy known as X-ray fluorescence. This release of energy is illustrated in Figure 7. This energy is determined by the different energies between the initial and final orbitals of the individual's electron transitions. The amount of element present in an object is determined by the intensity of the signal detected at its signature energy.

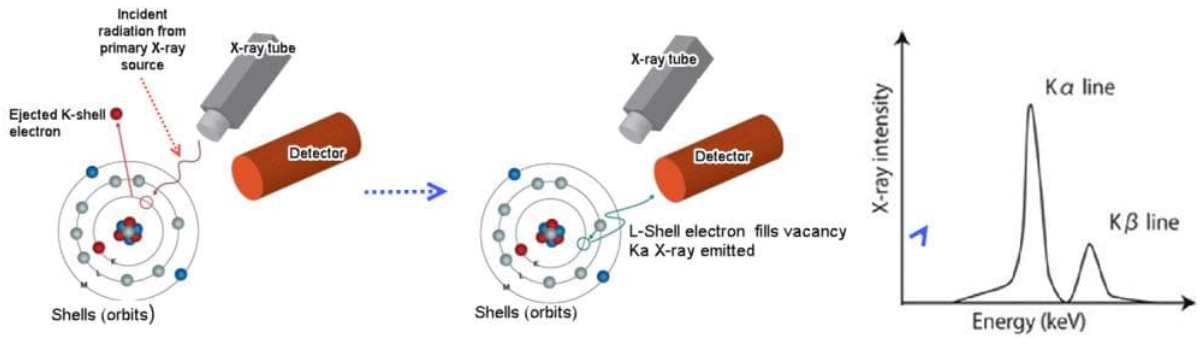

Figure 7. The mechanism of characteristic X-ray generation.

Standard µXRF configuration is presented in Figure 8. The sample can be scanned to measure the elemental distribution within a sample with a spatial resolution as small as 10 µm (energy dependent).

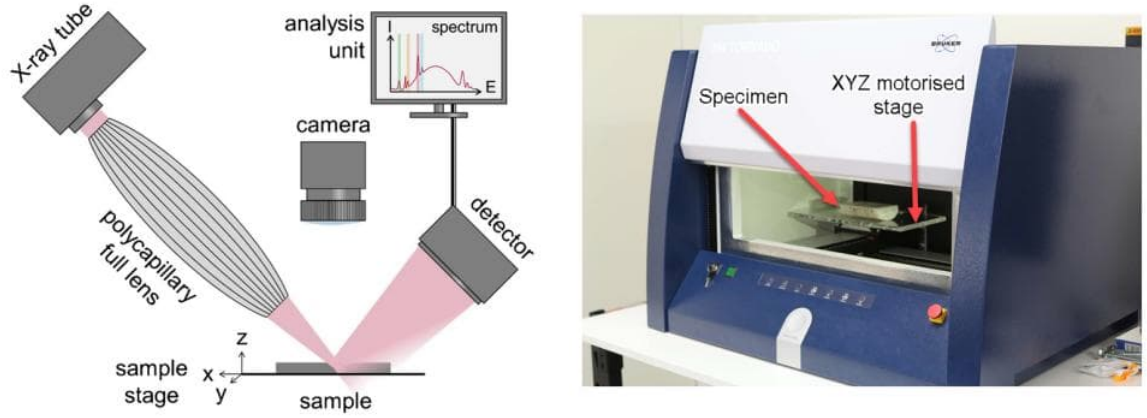

Figure 8. Schematic showing the main components of the Micro X-ray Fluorescence (µXRF) [14].

Micro-XRF allows for fast measurements of large areas, with high spatial resolution in short times. The individual element distributions can be visualized and extracted quickly. Fundamental parameter-based quantification allows for a quick assessment of the composition of the sample. Smart analysis of mapping allows for semi-quantitative analysis of complex chemical compounds concentration in the concrete matrix.

As an example, presented in Figure 9, drawing out a series of objects allows for semi-quantitative analysis: The HyperMap data can be used to tell the aggregates apart from the cement and quantify the cement composition into the depth of the sample. In this example, the Cl concentration goes from 1 wt.% to 0 wt.% within the first 10 mm. The K concentration is anticorrelated to the Cl (leaching). The sum of SiO2 and CaCO3 is stable at about 85 wt.%.

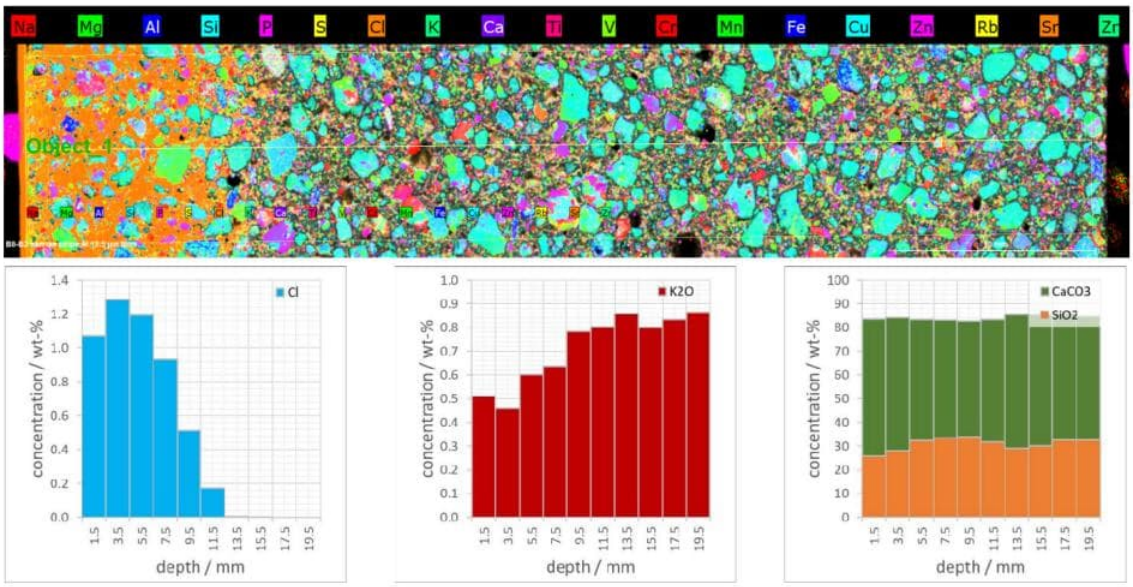

Figure 9. Examples of the Micro X-ray fluorescence (micro-XRF) distribution maps of some chemical compounds in concrete [15].

3.2 Measurement of chloride profiles – Potentiometric titration

Chloride titrations are carried out to determine the ingress of chloride ions of the concrete surface. The measurement of chloride profiles is determined by applying the standard m EN 14629 (Products and systems for the protection and repair of concrete structures - Test methods - Determination of chloride content in hardened concrete, method B, potentiometric titration). The potentiometric titration belongs to chemical methods of analysis in which the endpoint of the titration is monitored with an indicator electrode that records the change of the potential as a function of the amount (usually the volume) of the added titrant of exactly known concentration.

Figure 10. Example of the potentiometric titrators used in the titration method.

Chloride content analyses is performed from specimens by grinding powder samples as presented in Figure 11. The titration samples are ground from the concrete specimens at the following depths:

- Sample 1. From a depth of 0 to 3 mm
- Sample 2. From a depth 5 to 8 mm
- Sample 3. From a depth of 10 to 13 mm
- Sample 4. From a depth of 15 to 18 mm
- Sample 5. From a depth of 20 to 23 mm
- Sample 6. From a depth of 28 to 31 mm
- Sample 7. From a depth of 38 to 41 mm
- Sample 8. From a depth of 48 to 50 mm

The Profile Grinder, presented in Figure 11, is used to obtain concrete powder samples at small depth increments for accurate determination of chloride ion profiles. The Profile Grinder grinding machine, pulverizes the concrete into a fine powder at exact depth

increments, which can be selected between 0.5 mm to 2.0 mm. The grinding area is 73 mm in diameter and the maximum depth is 40 mm. For every depth increment of 1 mm, approximately 9 grams of powder is obtained for analysis.

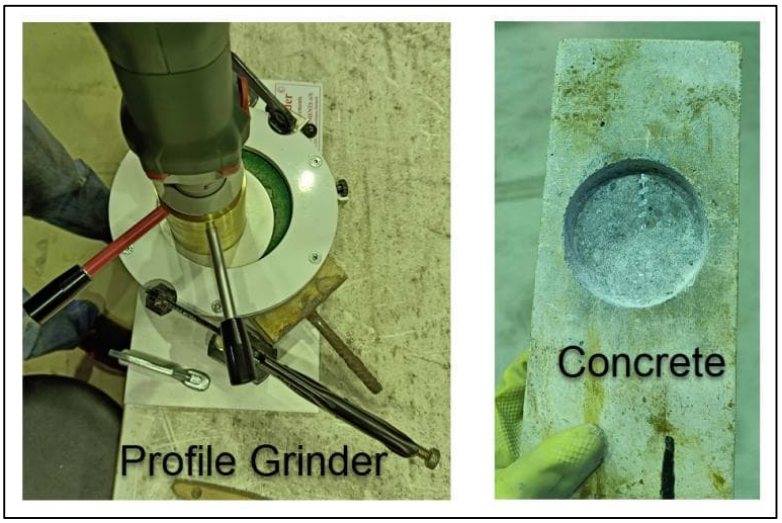

Figure 11. Concrete sampling for chloride measurement – Profile grinder.

According to the standard, the minimum weight of the powder sample should be approx. 10 g. The chloride content is determined with 0,1 M silver nitrate solution in a potentiometric titration. Consumption of silver nitrate solution (V3) in the titration is noted. The first derivative method is to be used. First derivative is a technique of adding small aliquots of titrant to the sample, recording the potential changes, and applying a first derivative analysis to the data, from which the endpoint is calculated. The technique assumes that the change in mV reading per volume of titrant added will be greatest at the endpoint. The chloride content of the concrete as percent of chloride ion is calculated by mass of sample using the following formula:

$$Cl\% - wt\ of\ concrete = \frac{3{,}545 * f * V_3}{m} * 100 \quad (3)$$

Where (f) is the molarity of silver nitrate solution, (V_3) is the volume of the silver nitrate solution used in the titration [ml] and (m) is the mass of the concrete sample [g].

The chloride content by mass of cement is calculated using the following formula

$$Cl\% - wt\ of\ cement = Cl\% - wt\ of\ concrete * \frac{mass\ of\ concrete\ ingredients\ in\ kg}{mass\ of\ cement\ in\ kg} \quad (4)$$

3.3 Petrographic analysis – Thin Section Analysis

Thin Section Analysis (TSA) is a form of petrographic testing that is done to analyse the physical and chemical properties of materials. It is a typical testing procedure for rock and geological purposes, which was then integrated for soils, concrete, and other materials. It is a microscopic test, in which an image is taken and analysed. This form of testing is widely used to identify the mineralogy of the tested samples in a small scale. The testing is conducted on thin slices obtained from the concrete specimen or drilled core, and the image taken is then analysed to get a visual insight into the concrete's internal condition. The results of the TSA can be both quantitative and qualitative.

Concrete testing with TSA is done by slicing off very thin sections (around 30μm) of concrete from the specimen, which are then grinded and (if necessary) polished. The samples are then observed with a microscope to determine its physical properties. The obtained results, however, mainly depend on the experience of the tester, since a lot of the obtained information are qualitative. Figure 12 shows some preparation steps for the TSA analysis.

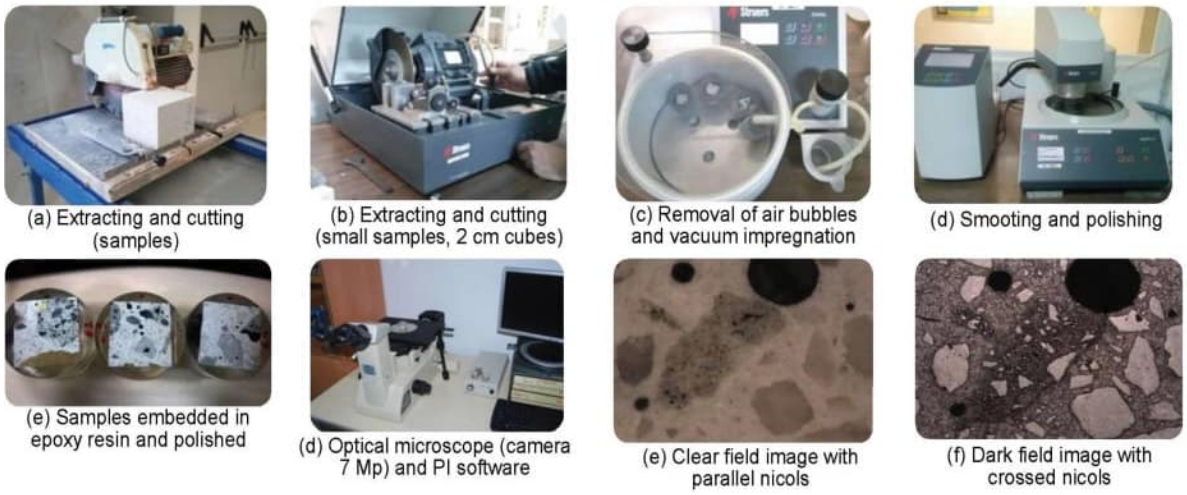

Figure 12: Sample preparation for optical petrographic analysis [16].

Based on the analysis of thin sections a long series of parameters and properties can be described, among those:

- aggregate distribution inside the concrete (as well as size and quality of those aggregates),
- the existence of cracks in the concrete's microstructure (their size, and the cause of the cracks),
- the presence and extent of damage in the concrete as well as the cause of that damage
- the air content in the concrete's pore structure
- the existence of different binder materials, as well as signs of expansive ettringite formation, AAR, and sulphate damage.
- w/c-ratio and homogeneity of cement paste
- Cement type and content
- Cement hydration and content of microcracks

- Bleeding and paste stability while the concrete was still plastic
- Bonding quality and ITZ for paste-sand and paste-stone.
- Degree of carbonation

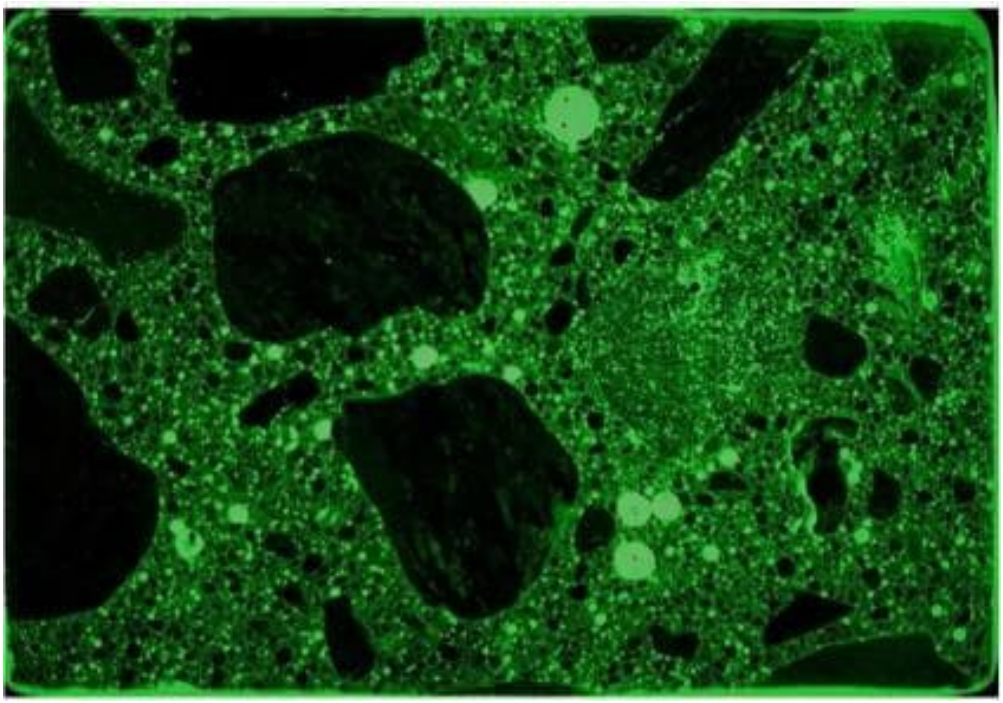

Figure 13. Example of this-section analysis. A 20µm thick fluorescence impregnated thin section in uv-light. The dimensions are 45mm x 30mm x 0.020mm.

4. Results and discussion

4.1 Chemical analysis of concrete samples

The chemical analysis of concrete samples was performed using two different techniques:

1) Micro-XRF analysis
2) Potentiometric chloride titration method

Micro-XRF analysis

Utilizing scanning micro-XRF analysis, we examined the 2D surface characteristics of 9 concrete samples, presented in Figure 14. This analysis produced intensity elemental maps, providing valuable information on the distribution patterns of different elements within the samples. The maps include detailed representations of both major and minor elemental distributions, along with F1 (free energy ranges comparable to backscatter images) to improve clarity. Line scans depicting the distribution of Mg, Ca, and S along the samples are also presented. Additionally, a separate Excel sheet containing elemental data is provided.

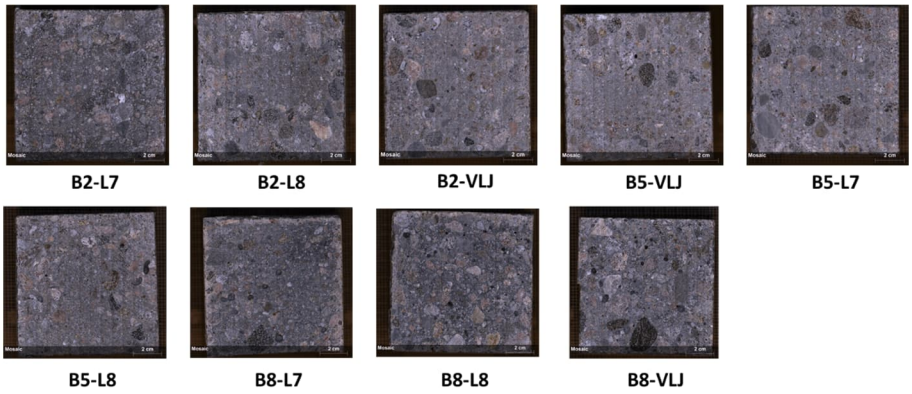

Figure 14. Concrete samples examined by micro-XRF.

Analyses were obtained with a Bruker M4 Tornado plus (with AMICS) at the Geological Survey of Finland (GTK). The system has an Rh X-ray 30-Watt Rh anode target, two simultaneously operating 30mm2 XFlash® silicon drift detectors (SDD) with an energy resolution of < 145 eV at 275 kcps (measured on MnKα) via beryllium windows and poly-capillary optics.

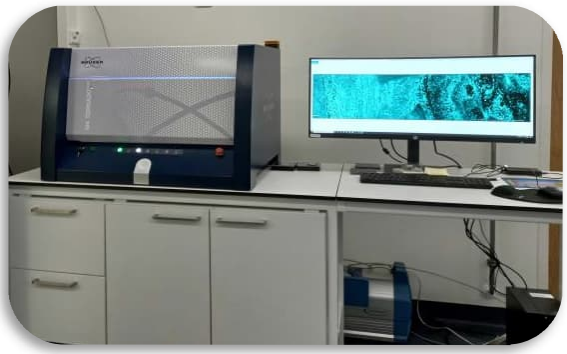

Figure 15. Bruker M4 Tornado plus (with AMICS) micro-XRF scanner.

Scanning and sample navigation is carried out via a motorized stage which moves the sample beneath the static X-ray beam. No sample preparation was needed. The accelerating voltage was 50 kV with a beam current of 600 µA, using a fixed spot size of 20 µm under 2 mbar vacuum. The samples were mapped in separate runs using a step size of 75 µm and a pixel dwell time of 5 ms. The qualitative elemental maps were generated using the Bruker M4 software.

Chloride titration

The chloride titration test was performed using the potentiometric titration method of the standard SFS-EN 14629:2007, using samples 5 different samples (Figure 16).

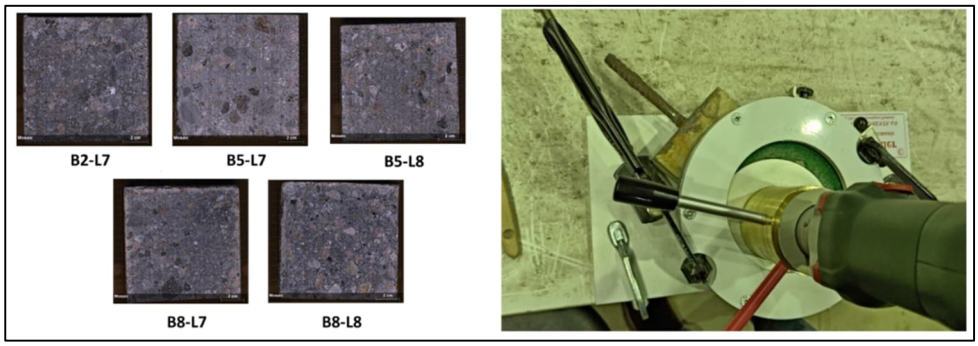

Figure 16: Profile grinder for chloride ingress samples.

A sufficient amount of powdered sample was drilled from the structural specimens from different depths as presented in Table 6. A profile grinder (shown in Figure 16) was used to obtain the powder samples. The specimen is locked in place and the grinder is used to obtain powder samples (max 1 mm at a time) from the surface of the concrete. The grinded dust is collected and stored in separate containers for each tested depth.

Table 6: Depth of powder samples for chloride penetration testing.

Sample (per specimen)	Depth range
1	0-3 mm
2	5-8 mm
3	10-13 mm
4	15-18 mm
5	20-23 mm
6	28-31 mm

The chloride content of the sample was measured by the weight of concrete. In different sources, the chloride threshold that is usually used is around 0.4% by weight of the binder [17]. Threshold chloride concentration values vary but are typically in the range of 0.05 to 0.1% by weight of concrete. Chloride limits are expressed on the basis of the weight of Portland cement. These threshold chloride values can be approximated to about 0.4 to 0.8% by weight of cement.

In this case, however, the concrete for most of its service life (in which chloride corrosion can occur) is submerged under groundwater. In this situation, the risk and the rate of corrosion is lower (the surrounding environment is anaerobic). The chloride threshold in this case can be taken as 2.2% by cement weight [18]. This value is based on testing, and the

actual threshold can differ based on specific storage conditions. Based on the previous iterations of this project, the ratio of cement in the concrete by weight is 0.155 [19].

4.1.1 Sulphate profiles

The sulphate content profiles measured by micro-XRF for concretes B2, B5 and B8 in water solutions L7, L8 and VLJ groundwater are presented in Table 7. The corresponding figures are presented in Figure 17. The acid soluble sulphate content is expressed as the total sulphate ions (SO_4^{2-}) by the weight of concrete. Sulphate tests were not performed for the concrete sample B5/L7.

Table 7. Sulphate profile contents as a function of concrete depth.

	Sulphate content % ($SO4^{2-}$) by wt. of concrete								
Depth [mm]	B2/L7	B2/L8	B2/VLJ	B5/L7	B5/L8	B5/VLJ	B8/L7	B8/L8	B8/VLJ
0-3	0,02	0,03	0,11		0,08	0,18	0,17	0,14	0,13
5-8	0,02	0,03	0,07		0,12	0,12	0,12	0,13	0,12
10-13	0,03	0,03	0,07		0,10	0,17	0,13	0,13	0,11
15-18	0,04	0,04	0,09		0,12	0,12	0,13	0,14	0,12
20-23	0,04	0,05	0,06		0,16	0,11	0,11	0,15	0,08
28-31	0,06	0,06	0,10		0,19	0,10	0,10	0,15	0,09

** The sulphate ion (SO_4^{2-}) concentrations are: 20 mg/L in L7, 500 gm/L in L8 and 45 mg/L in VLJ solutions.*

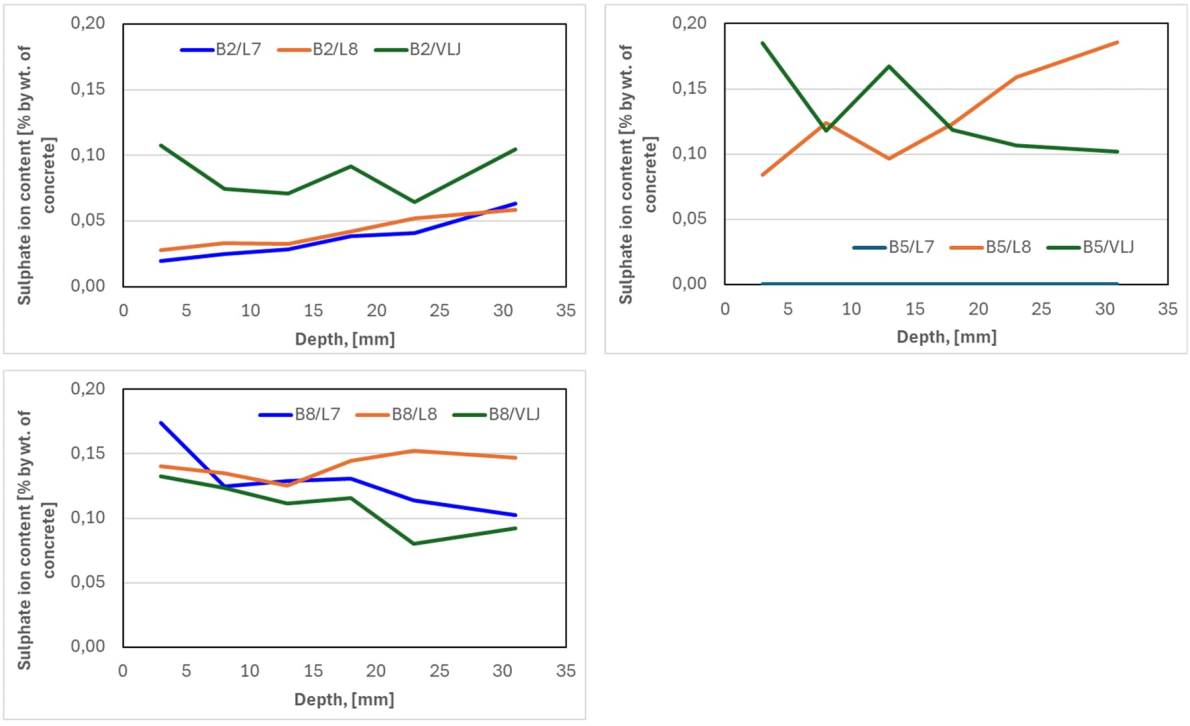

Figure 17. Sulphate profiles for concrete specimens.

The sulphate profiles obtained by the micro XRF analysis of the samples were relatively low, and the values were, for the most part, sporadic. This makes it difficult to determine whether the sulphates observed were ingress or from the original mix materials. Overall, the

sulphate content seems, as expected, to be a bit higher in B8 and B5 concretes, which is made using slag and silica fume respectively. The values for the most part, did not show a pattern (sulphate values does not decrease with depth, not higher in the surfaces). In the petrographic analysis of the samples, there was no indication of any damage due to sulphate attacks.

The micro-XRF measuring head is mounted on a remote-controlled X-Y-Z stage which enables to execute high spatial resolution line-scan and area mapping providing multi-element analyses on areas with maximum dimensions of 75×75mm2. Element distributions across the sample are then originated by dedicated software. The details of the measurement line-scan of the sulphate profiles are presented in Figure 18 and the area mapping is presented in Appendix (A).

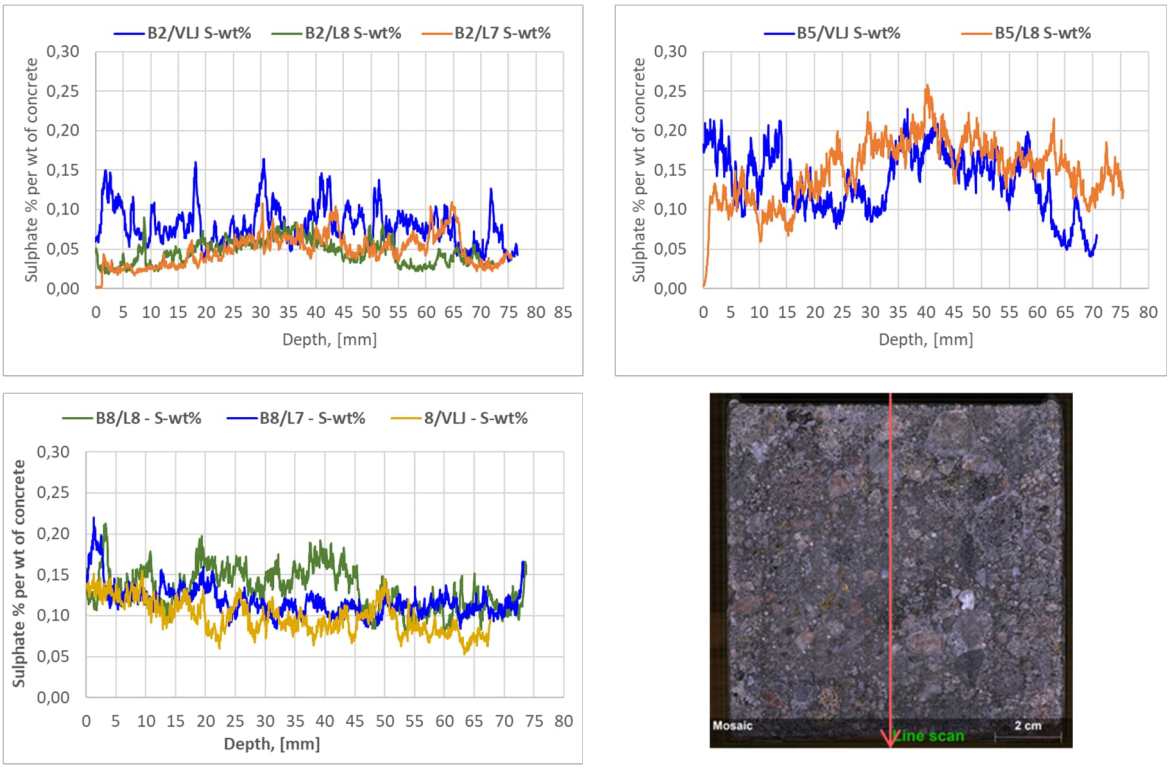

Figure 18. Details of the sulphate profiles of the different concrete samples.

4.1.2 Magnesium profiles

The magnesium content profiles for concretes B2, B5 and B8 in water solution L7, L8 and VLJ groundwater are presented in Table 8. The corresponding graphs are presented in Figure 19. The acid soluble magnesium content is expressed as the total magnesium (Mg) by the weight of concrete. Magnesium tests were not performed for the concrete sample B5/L7.

Table 8. Magnesium contents as a function of concrete depth.

	Magnesium content % (Mg) by wt. of concrete								
Depth [mm]	B2/L7	B2/L8	B2/VLJ	B5/L7	B5/L8	B5/VLJ	B8/L7	B8/L8	B8/VLJ
0-3	0,12	0,23	0,25		0,23	0,34	0,84	0,91	0,82
5-8	0,18	0,21	0,25		0,30	0,38	0,72	0,78	0,83
10-13	0,21	0,21	0,23		0,33	0,34	0,76	0,78	0,78
15-18	0,19	0,22	0,24		0,39	0,40	0,81	0,87	0,75
20-23	0,22	0,40	0,25		0,33	0,34	0,75	0,85	0,85
28-31	0,23	0,32	0,25		0,35	0,49	0,68	0,84	0,66

** The Magnesium ion (Mg) concentrations are: 50 mg/L in L7, 100 gm/L in L8 and 0,16 mg/L in VLJ solutions.*

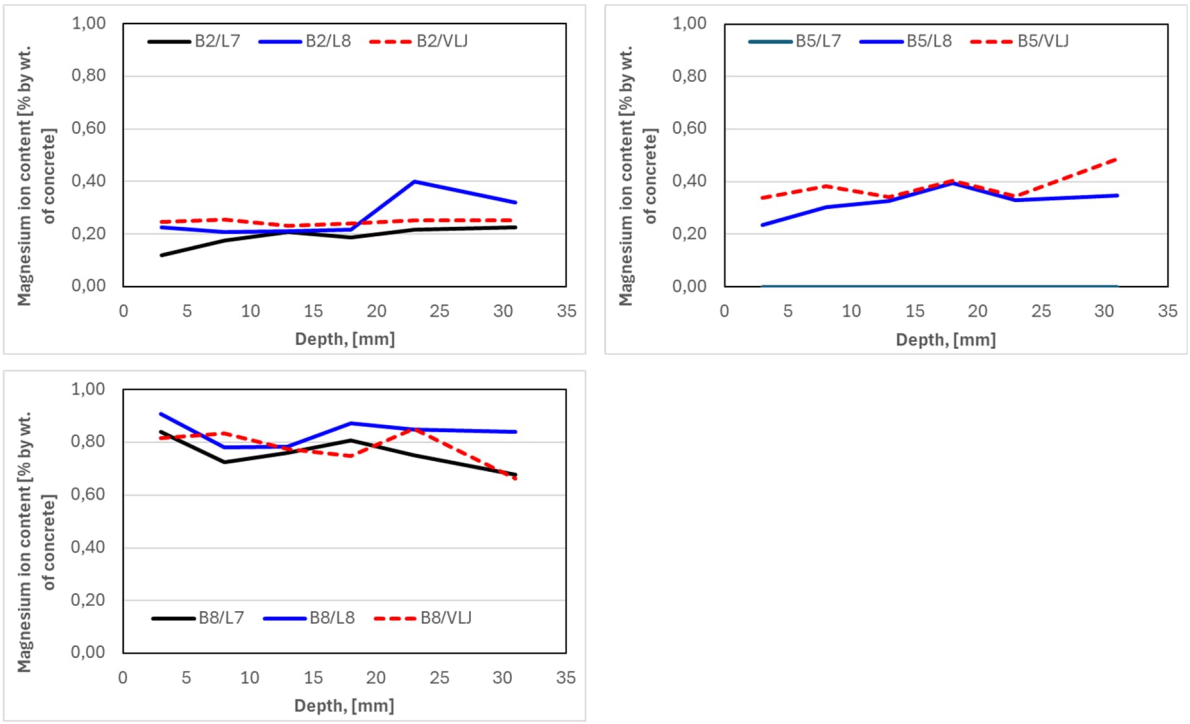

Figure 19. Magnesium profiles for concrete specimens.

Based on the results of the magnesium micro XRF analysis, it can be seen that the concrete specimens that were made with GBFS binder (B8) generally have much higher magnesium content compared to the other samples under all storage conditions. This is expected, due to the slag having high-er magnesium content in its mineral phases. Overall, similar to the sulphate profiles, the results did not show any noticeable trend, and the charts obtained have been flat for the most part (the values are not higher on the surface for example). This makes it difficult to justify whether the magnesium content is ingress or if it is from the mix

materials. By using the micro XRF method, the content of magnesium in general is determined, but determining the mineral phases that it exhibits is not, which also complicates this procedure. The values are, in general, relatively low. The details of the measurement line-scan of the magnesium profiles are presented in Figure 20 and the area mapping is presented in Appendix (A).

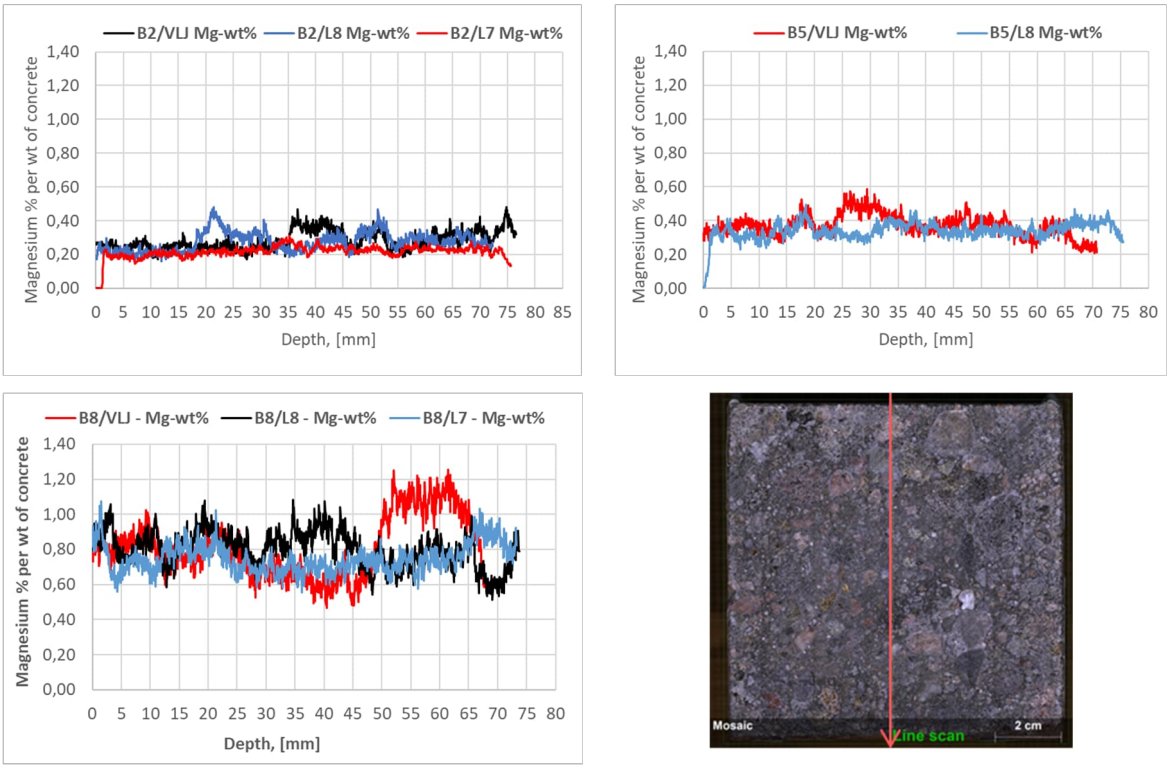

Figure 20. Details of the magnesium profiles of the different concrete samples.

4.1.3 Chloride profiles

The chloride content profiles for concretes B2, B5 and B8 in water solutions L7 and L8 are presented in Table 9. The acid soluble chloride content is expressed as the total chloride (Cl^-) by the weight of concrete. Chloride tests were not performed for the concrete samples B2/L8, B2/VLJ, B5/VLJ and B8/VLJ solution as there was no powder samples for these concretes.

Based in the previous research performed by Ba Ragaa (2023) [2], the obtained results for samples stored in groundwater show the very low values obtained for chloride penetration into the samples. All the test-ed samples in all specimens did not show any sign of chloride attack, as all the tests had a chloride content that is smaller than 0.01% per weight of concrete. With these low margins, it is safe to assume that under normal circumstances in groundwater conditions, there will be no damage done due to chloride attacks, and there should be no chloride induced corrosion for this storage period.

Table 9. Chloride contents as a function of concrete depth.

Depth	Chloride % (Cl-) by wt. of concrete				
	B2-L7	B5-L7	B5-L8	B8-L7	B8-L8
1 – 3 mm	< 0,01	0,01	0,04	0,01	0,03
3 – 5 mm	0,01	< 0,01	0,03	< 0,01	0,02
5 – 8 mm	< 0,01	< 0,01	0,03	< 0,01	0,01
10 – 13 mm	0,01	< 0,01	0,02	< 0,01	< 0,01
15 – 18 mm	< 0,01	< 0,01	0,02	< 0,01	< 0,01
20 – 22 mm	< 0,01	< 0,01	0,01	< 0,01	< 0,01

** The Chloride ion (Cl^-) concentrations are: 50 mg/L in L7, 1000 gm/L in L8 and 17 mg/L in VLJ solutions.*

In the samples stored in solution L8, chloride penetration has been detected across the samples. The B5/L8 samples tend to show the highest risk of chloride attacks, and their relative chloride penetration is fairly high compared to the other specimens. The chloride ingress through the specimen is relatively high deep inside the concrete's microstructure. The other specimens, B2 and B8 are showing smaller chloride content past the 15 mm depths. The B8 specimen has a high peak in the second sample at 1 – 3 mm depth, but the obtained chloride content past the 20 mm range is considered to be of lower risk. The values obtained here are lower than the determined threshold (0.34%) for submerged concrete in anoxic environments.

4.2 Microstructure analysis – petrographic analysis (thin-sections)

Petrographic analysis was performed to acquire information about the microstructure of the concrete specimens after 27 years storage in different salt solutions. The results obtained from the petrographic analysis were, for the most part, qualitative. The petrographic images were used to evaluate various parameters such as cement type, the presence and depth of carbonation, the existence of cracks (and if present, the severity of those cracks), the porosity of the sample, as presented in Table 10. The conducted testing and evaluation can also showcase local parameters that are present in a specific sample. Overall, the results obtained are judged qualitatively based on experience.

Table 10. Summary of the petrographic thin-section analysis. The results are based on both the observations and the interpretation made by the petrographer.

Sample	Depth	Average carbonation depth*	Compaction**	Quality	Deterioration
B2 L7	0–43 mm from the cut bottom surface	0 mm	3	Normal	NO
B2 L8	0–43 mm from the cut bottom surface	0 mm	3	Normal	NO
B2 VLJ	0–47 mm from the cut top surface	0 mm	3	Normal	NO
B5 L7	0–41 mm from the cut top surface	0 mm	3	Some defects	NO
B5 L8	0–42 mm from the cut top surface	1 mm	3	Some defects	NO
B5 VLJ	0–45 mm from the cut bottom surface	0 mm	3	Some defects	NO
B8 L7	0–47 mm from the cut top surface	0 mm	3	Some defects	NO
B8 L8	0–47 mm from the cut top surface	5,5 mm*	3	Some defects	NO
B8 VLJ	0–33 mm from the cut top surface	0 mm	3	Some defects	NO

*The depth of carbonation has been measured from the cut surface.
** Compaction is given on scale 5 = very good, 4 = good, 3 = medium, 2 = poor, 1 = very poor

4.2.1 General summary

The samples were cut concrete test cubes. There was variation of composition between specimen set B2, B5 and B8. Also, some compositional differences were observed inside the concrete specimen set B8. The quality of the concrete samples was normal within the specimen set B2, some defects were observed among the other samples, such as unoriented microcracking and slightly weakened adhesion between the aggregate and paste. All the samples (B2, B5 and B8) were in anormal condition, and no distinct deterioration was detected.

4.2.2 Condition of aggregates

The aggregate consists mostly of granitoids, a few gabros, amphibolites and sandstones. Also, smaller quartz and feldspar grains were observed. The quality of the aggregate is normal, and it is mostly unaltered and intact. Sporadic adhesion cracks and air voids were observed between the aggregate and paste within the specimen specimens B5 and B8, but adhesion of the aggregates is mostly tight.

4.2.3 Condition of the cement paste

The cement paste was coarse-grained Portland Cement. The composition of the cement paste appeared to be different in every specimen set, presented in Figure 21.

- The paste contains eighter slag or small isotropic mineral particles in the specimen set B2.
- Within the set B5 the paste has slag, silica fume, fly ash and lime filler. Silica fume occurs as quite large lumps especially in the sample B5/L8.
- The paste of the samples within the set B8 contains lime filler and large amount of slag and small opaque particles, which could not be identified under the polarization microscope. In addition, small silica fume lumps were observed in the sample B8/VLJ. With that said and the similarity among the overall appearance of the cement paste of the specimen B8, it is possible that there is extremely fine silica fume also in the specimens B8/L7 and B8/L8.

The micro-texture of the cement paste was mostly homogenous, the microporosity is the highest in the specimen set B2 and the lowest in the specimen set B8. Otherwise, homogenous microporosity showed some variation within the specimen set B8, where the paste has higher porosity on the surface of some aggregates. There was only a diminutive carbonation near the top surface of the samples B5/L8 and B8/L8. However, it should be noted that the carbonation of the sample B8/L8 has been measured from the cut surface.

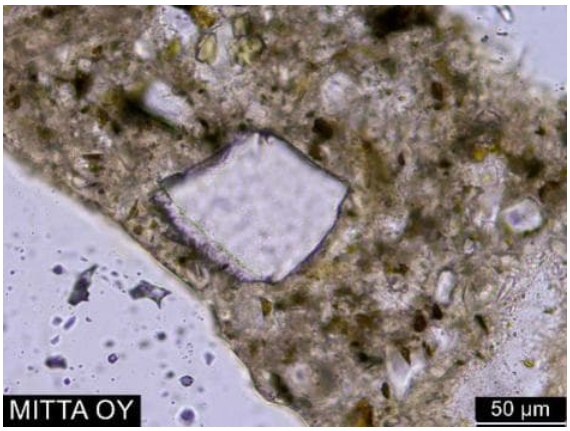

B2/L7 – Portland cement clinker and a slag resembling particle in the paste.

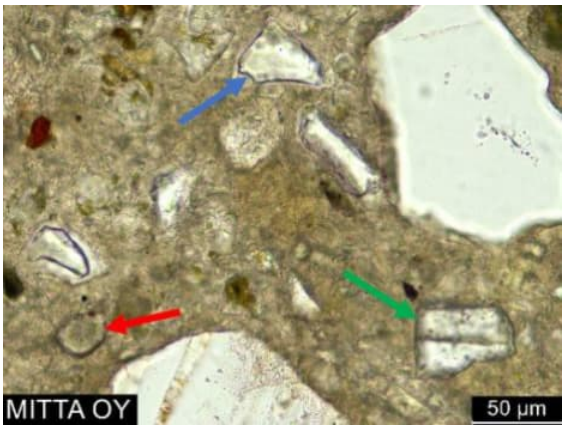

B5/L7 – The paste contains silica fume (red), slag (blue) and limestone filler (green).

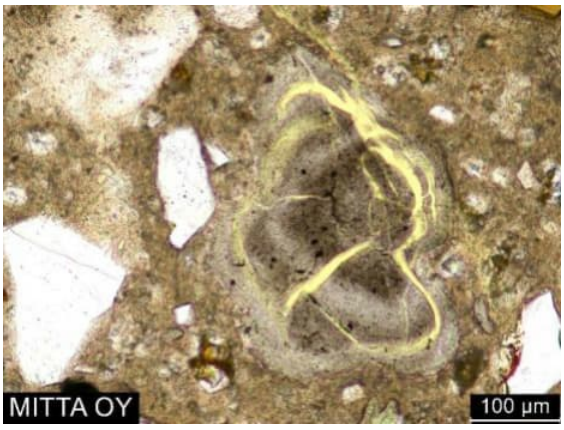

B5/L8 – A lump of silica fume

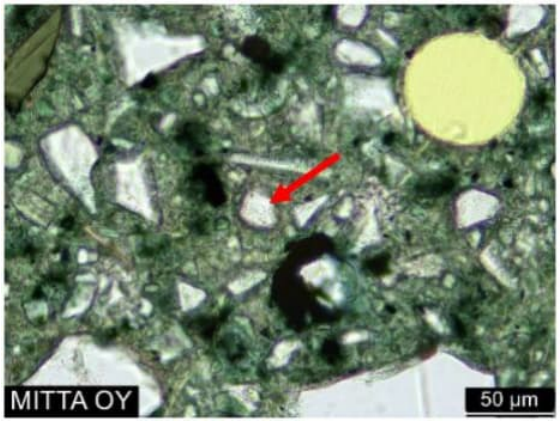

B8/L7 – The paste contains limestone filler (red) and abundantly slag particles (white and angular)

Figure 21. condition of the cement pastes in different specimen sets.

4.2.4 Air voids and compaction level

The air void content was only a visual estimation of the amount of round/spherical air voids Ø 0,02-0,8 mm (spacing factor > 0,30 = No, spacing factor < 0,30 = Yes). The Quality of the material is estimated on scale normal, some defects, significant defects. The condition of the sample is estimated on scale normal, impaired, significantly impaired. Deterioration (by weathering) is estimated on scale no deterioration, some indications, deteriorated.

The compaction of all samples was moderate. None of the concrete samples exhibited the desirable uniform structure of abundant, small, and spherical air voids, which were generally recognized to make a concrete durable to freeze-thaw.

4.2.5 Defects and deterioration

As presented in Figure 22, secondary ettringite related to water exposure was observed within the specimen sets B2 and B5. Based on the amount of ettringite and in the sample B2/L7 calcium hydroxide crystals observed in air voids, the most intense effect of moisture exposure was observed in the samples within the sample B2. In addition, there are thin

calcite crusts on the top surfaces of the samples B2/VLJ water and B5/L8, which indicates to the effect of moisture.

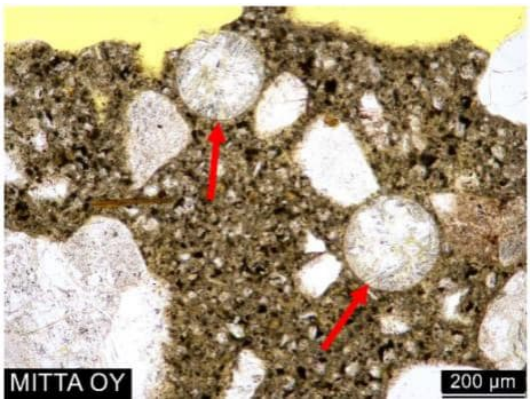

B2/L7 – Most of the smallest air voids (arrows) have been filled with ettringite near the cut bottom surface.

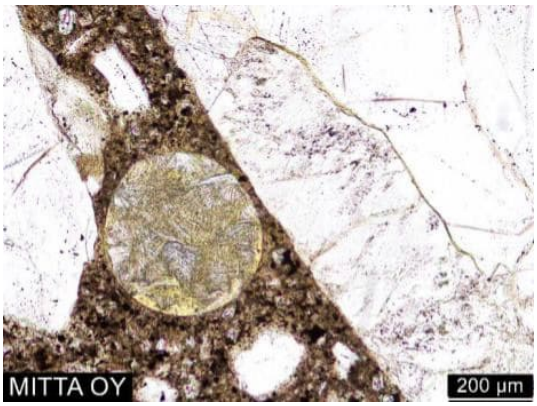

B2/L8 – Some of the smallest voids have almost been filled with ettringite crystals.

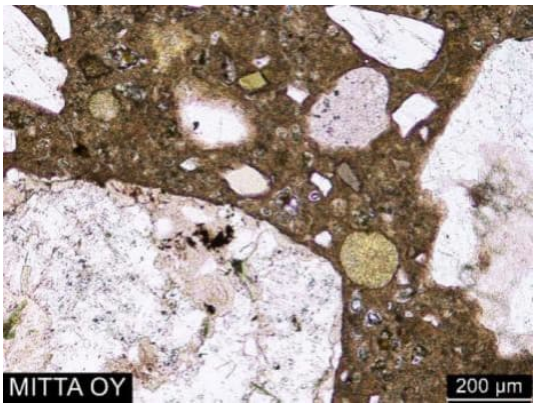

B5/L8 – Ettringite crystals in the air voids

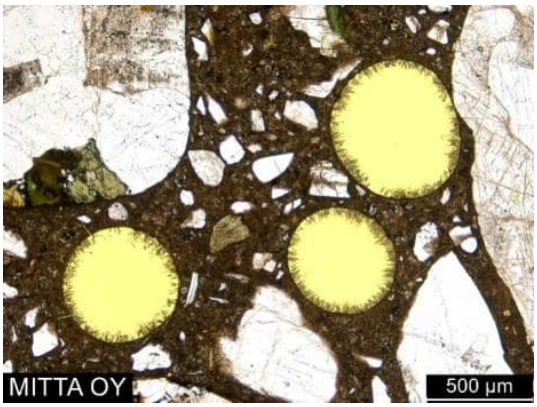

B5/VLJ – Ettringite crystals in slightly larger air voids.

Figure 22. Secondary ettringite formation in the B2 and B5 concrete specimens.

Unoriented microcracking was observed in all the samples. The intensity of the cracking was weakest within the specimen set B2 and the strongest within the specimen set B8. The cracking is most likely caused by shrinkage.

There were few cases especially within the specimen sets B5 and B8 where cracking cuts aggregates, but they can also be due to weakness zones in the aggregates themselves.

Some very delicate microcracking had proceeded in the paste form the reacted silica fume lumps, but the cracking was observed only very close to the lumps. No distinct signs from alkali-silica rection were observed.

The secondary crystallization of calcium hydroxide in the sample B2/L7 was most probably caused by paste leaching, but no leached paste was detected from the study area of the thin section. It is possible that the leached area is near the surface of the sample.

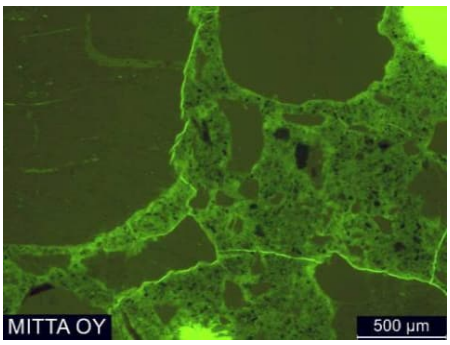

B2/L7 – Unoriented, quite weak microcracking

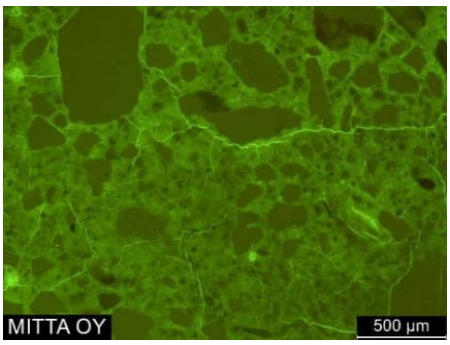

B5/L7 – Moderate to quite strong, unoriented microcracking.

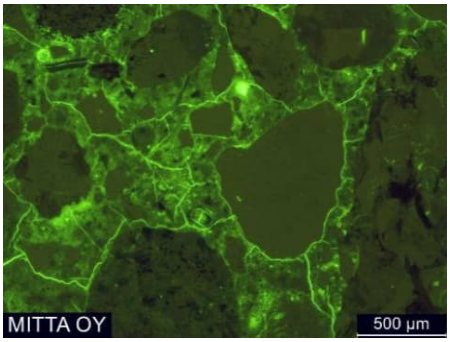

B5/L8 – Quite strong, unoriented microcracking

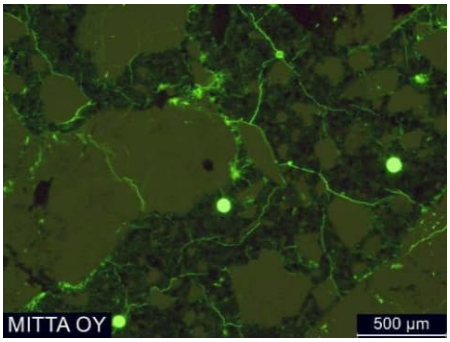

B8/L7 –Strong and unoriented microcracking.

Figure 23. Microcracking of concrete specimens.

4.2.6 Condition of the specimens coating

There was a double layered and maximum 0,15 mm thick coating on the top surface of the sample B5/L8. Based on its appearance under the polarization microscope, the upper layer of the coating is probably organic in composition. The lower layer resembles epoxy paint.

As presented in Figure 24, The top surface and three of the side surfaces of the concrete specimen B5/L8 were coated with glossy finished grey epoxy. One side surface was uncoated and darkened or stained concrete. The bottom surface was cut. One of the coating surfaces was detached the concrete specimen B5/L8.

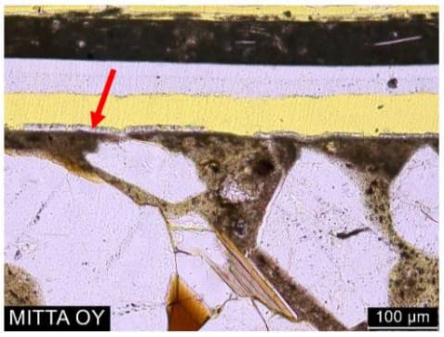

B5/L8 – Detached coating and a very thin calcite crust (arrow) on the top surface of the sample

B5/L8 – Epoxy coating

Figure 24. Coating condition of the B5/L8 specimen.

5. Summary

A joint project with nuclear power companies Fortum Power and Heat Oy and Teollisuuden Voima Oyj (TVO) was started in 1997 for acquisition of real data on long-term performance of concrete barriers in nuclear waste depositories. Nine concrete qualities with three binders and three water-binder ratios and aggregates-binder ratios were included in the tests. The long-term tests for concrete specimens in various chemical water solutions resembling the ground water were investigated every 10 years.

In this research report three concrete mixtures (i) B2 with 100% CEM I 42,5 SR cement, (ii) B5 with 90% CEM II A 42,5 cement and 10% silica fume and (iii) B8 with 20% CEM I 42,5R cement, 75% KJ-400 blast furnace slag and 5% silica fume were investigated. The three concretes were stored in different solutions including different sulphate, magnesium and chloride concentrations. The storage solutions were (i) L7 (20 mg/L sulphate ions, 50 mg/L chloride ions and 5 mg/L magnesium ions), (ii) L8 (500 mg/L sulphate ions, 1000 mg/L chloride ions and 100 mg/L magnesium ions) and (iii) Olkiluoto ground water VLJ (45 mg/L sulphate ions, 17 mg/L chloride ions and 0,16 mg/L magnesium ions).

Chemical analysis of the concrete specimens was performed using the micro-X-ray fluorescence method for measuring the sulphate and magnesium profiles and the chloride titration method for measuring the chloride profile. The petrographic (thin section) analysis of the concrete specimens was used for analysing the microstructure of concrete.

The obtained chloride ingress results for the samples stored under different mix solutions were lower than the determined threshold (especially at a suitable concrete cover depth). The threshold value, however, could vary depending on different circumstances. The threshold value was chosen for cases where the concrete is submerged in anoxic environments.

From the micro XRF analysis, the magnesium and sulphate contents of the samples B2, B5 and B8 were analysed. The figures and obtained results were quite sporadic, and it is hard to say if the detected sulphate and magnesium content were ingress or from the mix compositions. The values were rather low and did not exceed the set amount.

The petrographic analysis shows that there is variation of composition between specimen sets B2, B5 and B8. Also, some compositional differences were observed inside the set B8. The quality of the concrete samples is normal within the specimen set B2, some defects were observed among the other samples, such as unoriented microcracking and slightly weakened adhesion between the aggregate and paste. All the samples are in normal condition, and no distinct deterioration was detected.

6. References

[1] E. Vesikari and P. Koskinen, “Durability of Concrete Barriers in Final Depositories of Nuclear Waste,” Espoo, Feb. 2012. Accessed: Aug. 27, 2023. [Online]. Available: http://kyt2014.vtt.fi/julkaisut/koskinen_et_vesikari_VTT_R_01185_12.pdf

[2] A. Ba Ragaa, “Long-term durability testing of concrete in low and intermediate level waste repositories.” Jun. 12, 2023. Accessed: May 17, 2024. [Online]. Available: https://aaltodoc.aalto.fi/items/9b04a157-3318-48bb-a80f-95624c69e42a

[3] S. Mirvalad, “Improving performance of Portland-limestone cements in sulphate exposures using supplementary cementing materials,” 2013. Accessed: Apr. 14, 2022. [Online]. Available: https://www.researchgate.net/profile/Sajjad-Mirvalad/publication/326698202_Improving_performance_of_Portland-limestone_cements_in_sulphate_exposures_using_supplementary_cementing_materials/links/5fb28c3592851cf24cd6446e/Improving-performance-of-Portland-limestone-cements-in-sulphate-exposures-using-supplementary-cementing-materials.pdf

[4] “An Overview on Sulphate Attack.” Accessed: Apr. 12, 2022. [Online]. Available: https://www.ctlgroupqatar.com/single-post/2019/06/30/an-overview-on-sulphate-attack

[5] M. Mainguy, C. Tognazzi, J. M. Torrenti, and F. Adenot, “Modelling of leaching in pure cement paste and mortar,” *Cem Concr Res*, vol. 30, no. 1, pp. 83–90, 2000, doi: 10.1016/S0008-8846(99)00208-2.

[6] M. Moranville, S. Kamali, and E. Guillon, “Physicochemical equilibria of cement-based materials in aggressive environments—experiment and modeling,” *Cem Concr Res*, vol. 34, no. 9, pp. 1569–1578, Sep. 2004, doi: 10.1016/J.CEMCONRES.2004.04.033.

[7] E. Rozière *et al.*, “Durability of concrete exposed to leaching and external sulphate attacks,” *Cem Concr Res*, vol. 39, no. 12, pp. 1188–1198, Dec. 2009, doi: 10.1016/J.CEMCONRES.2009.07.021.

[8] O. O. Metalssi *et al.*, “Understanding the degradation mechanisms of cement-based systems in combined chloride-sulphate attack,” *Cem Concr Res*, vol. 164, p. 107065, Feb. 2023, doi: 10.1016/J.CEMCONRES.2022.107065.

[9] X. Yu, S. Li, J. Zheng, X. Chang, Y. Liao, and D. Chen, “Degradation process of reinforced concrete under chloride and sulphate attack with and without electric field,” *Journal of Building Engineering*, vol. 78, p. 107588, Nov. 2023, doi: 10.1016/J.JOBE.2023.107588.

[10] D. Sun, Z. Cao, C. Huang, K. Wu, G. De Schutter, and L. Zhang, “Degradation of concrete in marine environment under coupled chloride and sulphate attack: A numerical and experimental study,” *Case Studies in Construction Materials*, vol. 17, p. e01218, Dec. 2022, doi: 10.1016/J.CSCM.2022.E01218.

[11] Finnsementti, “Cemet types (in Finnish and English).” Accessed: Nov. 23, 2018. [Online]. Available: https://finnsementti.fi/

[12] A. Ipatti, “Betonin pitkäaikaissäilyvyys loppusijoitusolosuhteissa. Työvaihe: yhteenveto koebetonin betoniteknisistä perusominaisuuksista.,” Vantaa, Dec. 2010.

[13] “What is XRF (X-ray fluorescence) and How Does it Work?” Accessed: May 18, 2024. [Online]. Available: https://www.thermofisher.com/blog/ask-a-scientist/what-is-xrf-x-ray-fluorescence-and-how-does-it-work/

[14] F. A. Wahid, “Characterising concrete using micro X-ray fluorescence (µXRF),” Imperial College London, London, 2016. Accessed: Jan. 26, 2024. [Online]. Available: https://spiral.imperial.ac.uk/bitstream/10044/1/55139/1/Abdul%20Wahid-F-2017-PhD-Thesis.pdf

[15] “Building materials - Concrete | Bruker.” Accessed: May 18, 2024. [Online]. Available: https://www.bruker.com/en/products-and-solutions/elemental-analyzers/micro-xrf-spectrometers/m4-tornado-plus/building-materials-concrete.html

[16] Z. Sánchez-Roldán, I. Valverde-Palacios, I. Valverde-Espinosa, and M. Martín-Morales, “Microstructural analysis of concretes manufactured with recycled coarse aggregates pre-soaked using different methods,” *Materiales de Construccion*, vol. 70, no. 339, Sep. 2020, doi: 10.3989/MC.2020.16919.

[17] E. Vesikari and P. Koskinen, “Durability of Concrete Barriers in Final Depositories of Nuclear Waste,” 2012.

[18] U. M. Angst, O. B. Isgor, C. M. Hansson, A. Sagüés, and M. R. Geiker, “Beyond the chloride threshold concept for predicting corrosion of steel in concrete,” *Appl Phys Rev*, vol. 9, no. 1, p. 011321, Mar. 2022, doi: 10.1063/5.0076320.

[19] A. Ipatti, “Betonin pitkäaikaissäilyvyys loppusijoitusolosuhteissa ,” 2010.

7. Appendices

7.1 Appendix (A) – micro XRF measurement data

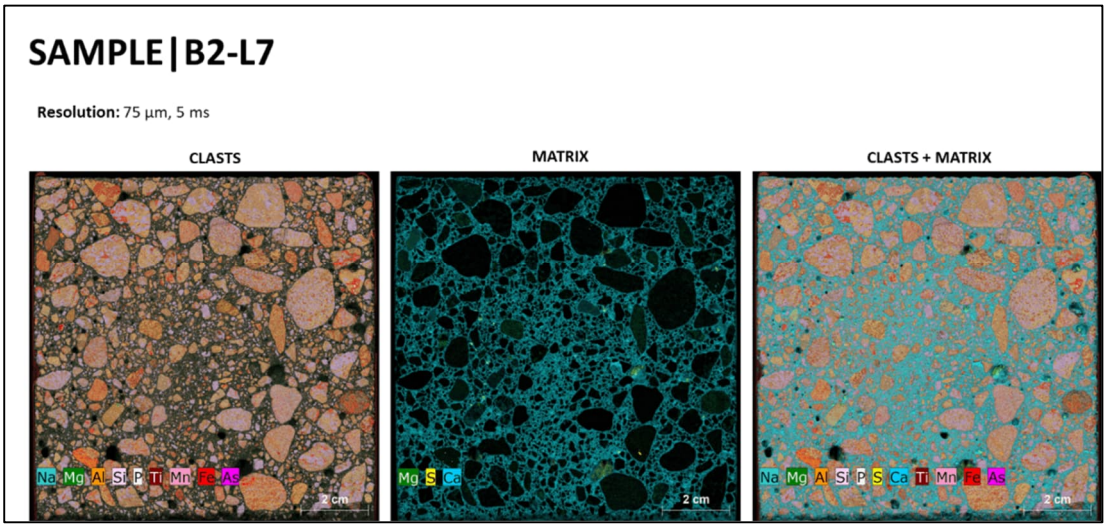

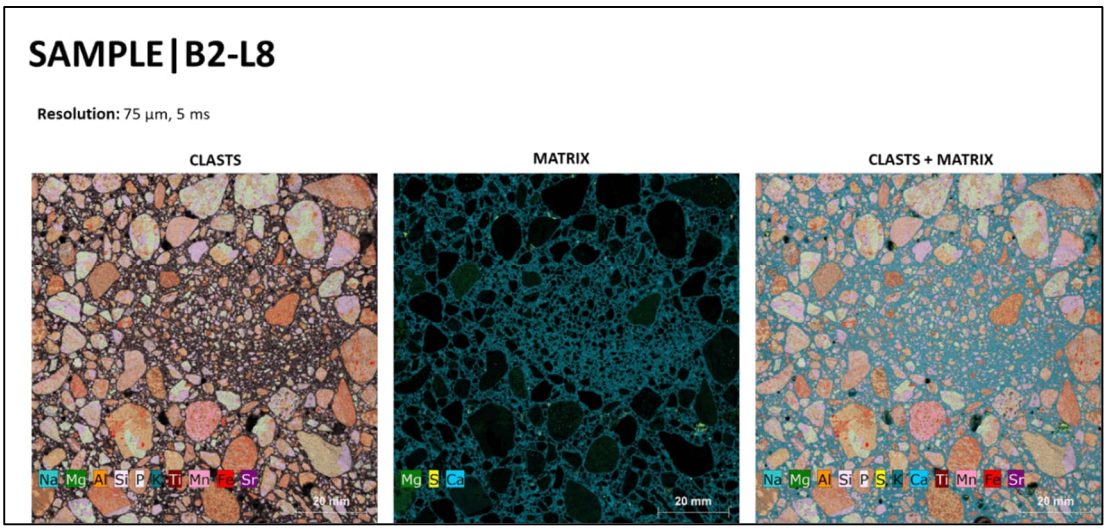

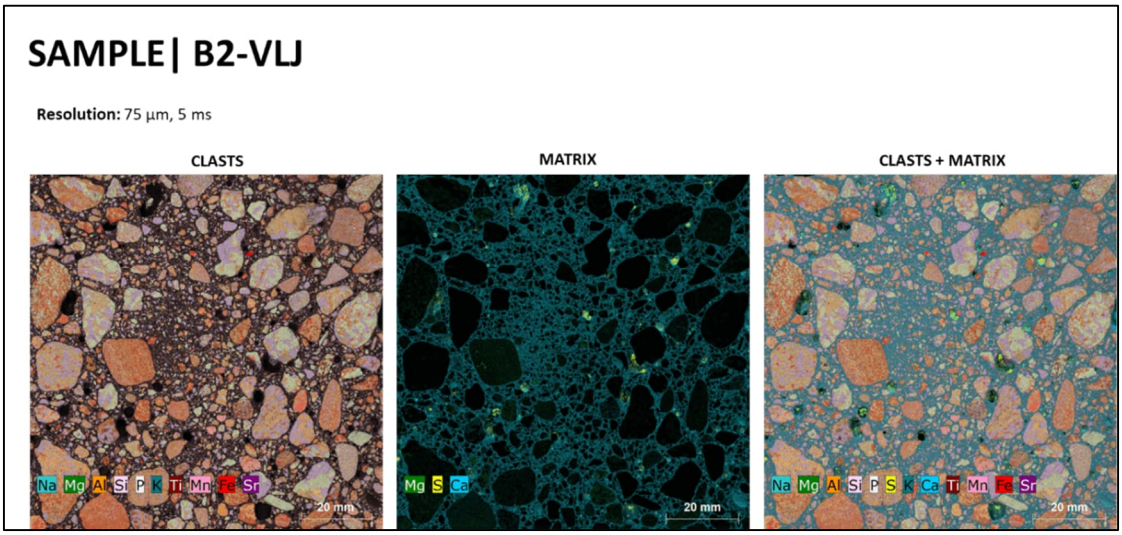

SAMPLE| B5-L7

Resolution: 75 µm, 5 ms

CLASTS

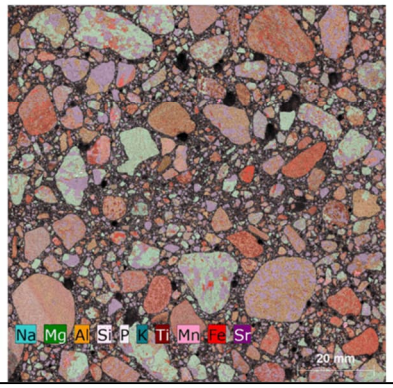

MATRIX

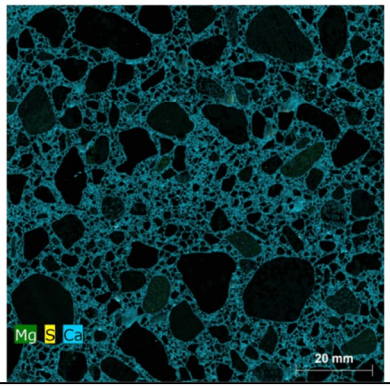

CLASTS + MATRIX

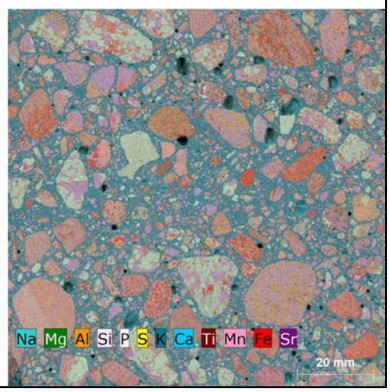

SAMPLE| B5-L8

Resolution: 75 µm, 5 ms

CLASTS

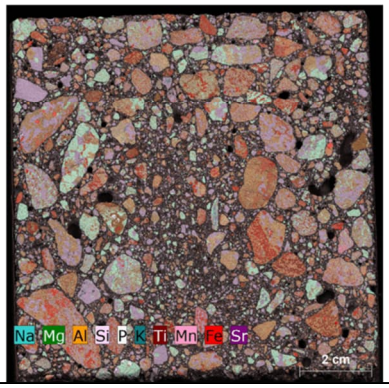

MATRIX

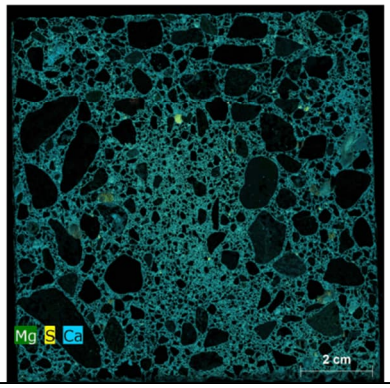

CLASTS + MATRIX

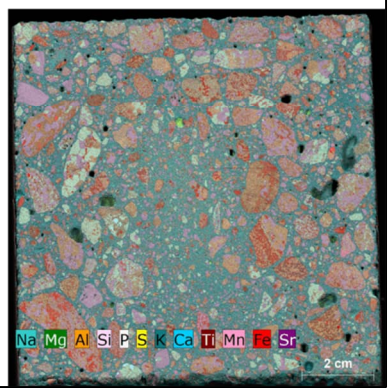

SAMPLE| B5-VLJ

Resolution: 75 µm, 5 ms

CLASTS

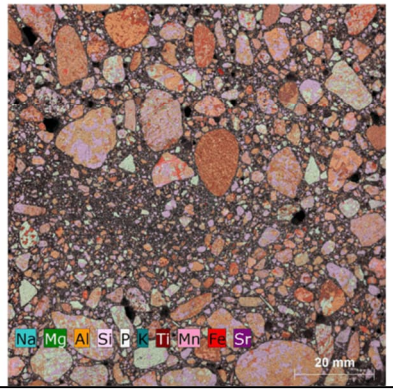

MATRIX

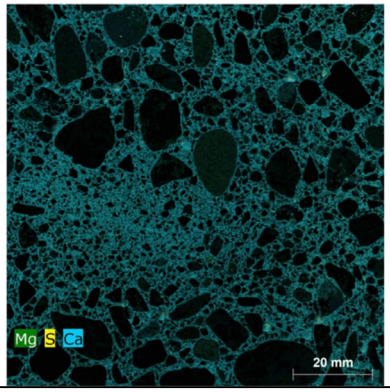

CLASTS + MATRIX

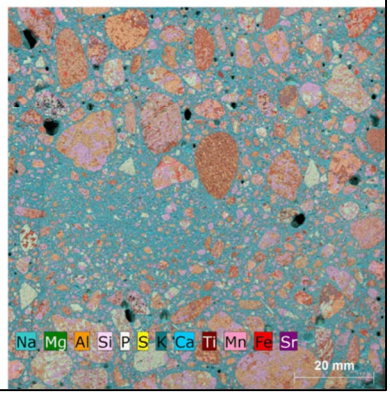

SAMPLE| B8-L7

Resolution: 75 µm, 5 ms

CLASTS

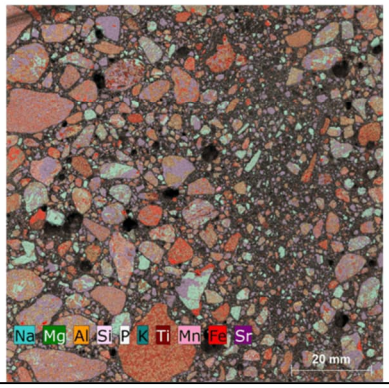

MATRIX

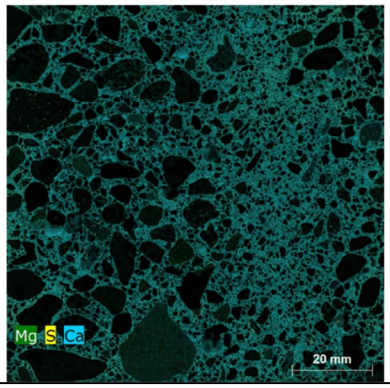

CLASTS + MATRIX

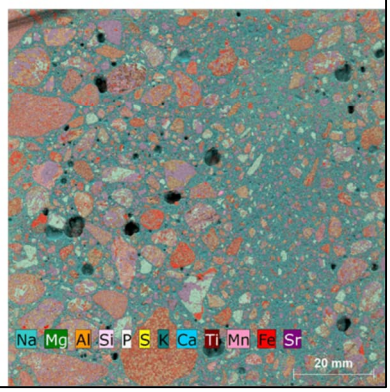

SAMPLE| B8-L8

Resolution: 75 µm, 5 ms

CLASTS

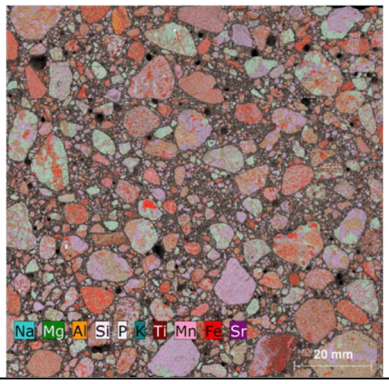

MATRIX

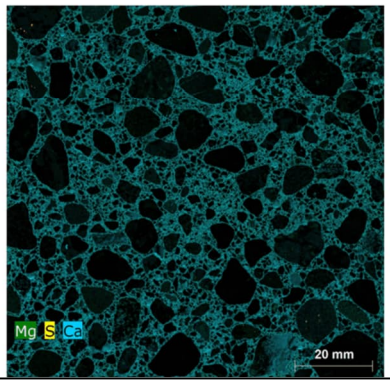

CLASTS + MATRIX

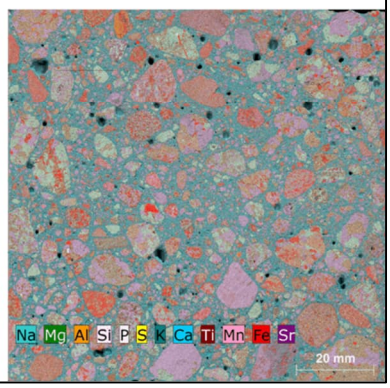

SAMPLE| B8-VLJ

Resolution: 75 µm, 5 ms

CLASTS

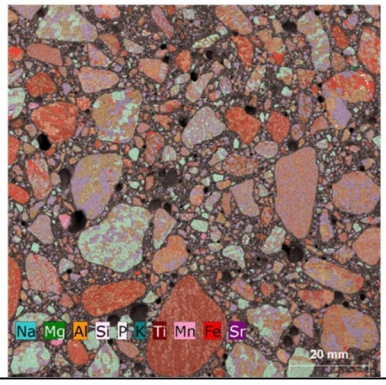

MATRIX

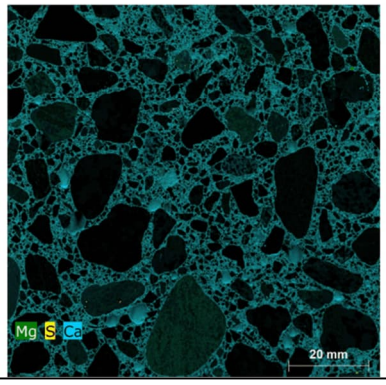

CLASTS + MATRIX

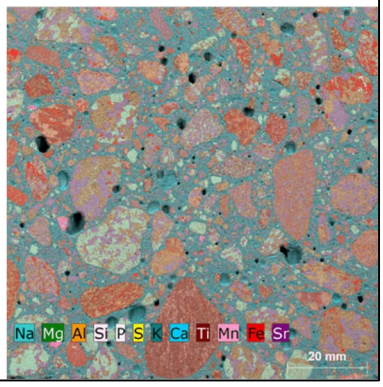

7.2 Appendix (B) – Chloride ingress report

MITTA

DETERMINATION OF CHLORIDE CONTENT

TEST REPORT CL 4917 | 09.04.2024

FINAS
Finnish Accreditation Service
T354 (EN ISO/IEC 17025)

ORDER INFO

Customer	Site	
Aalto-yliopisto	PERCO2 säilyvyyskappaleet (1998–2024)	
	Order data	Sample delivery date
	26.03.2024	26.03.2024
Distribution		
fahim.al-neshawy@aalto.fi		

TEST RESULTS

The detection limit for the measurements is 0.01 weight-% and the uncertainty (at a 95% confidence level) ± 0.01 weight-%. The measurements were performed on 8. - 9.4.2024. The sample ID, sample description, and sample type are information provided by the customer.

Sample ID	Sample description	Sample type	Analyzed sample mass [g]	Cl^- [weight-%]	Notes
B2-L7_0-3 mm		Powder	2.549	< 0.01	
B2-L7_3-5 mm		Powder	2.766	0.01	
B2-L7_5-8 mm		Powder	2.611	< 0.01	
B2-L7_10-13 mm		Powder	2.656	0.01	
B2-L7_15-18 mm		Powder	2.669	< 0.01	
B2-L7_20-22 mm		Powder	2.548	< 0.01	
B5-L7_0-3 mm		Powder	2.534	0.01	
B5-L7_3-5 mm		Powder	2.566	< 0.01	
B5-L7_5-8 mm		Powder	2.565	< 0.01	
B5-L7_10-13 mm		Powder	2.793	< 0.01	
B5-L7_15-18 mm		Powder	2.544	< 0.01	
B5-L7_20-23 mm		Powder	2.574	< 0.01	
B5-L8_0-3 mm		Powder	2.597	0.04	
B5-L8_3-5 mm		Powder	2.616	0.03	

Sample ID	Sample description	Sample type	Analyzed sample mass [g]	Cl^- [weight-%]	Notes
B5-L8_5-8 mm		Powder	2.588	0.03	
B5-L8_10-13 mm		Powder	2.511	0.02	
B5-L8_15-18 mm		Powder	2.501	0.02	
B5-L8_20-23 mm		Powder	2.528	0.01	
B8-L7_0-3 mm		Powder	2.542	0.01	
B8-L7_3-5 mm		Powder	2.549	< 0.01	
B8-L7_5-8 mm		Powder	2.524	< 0.01	
B8-L7_10-13 mm		Powder	2.568	< 0.01	
B8-L7_15-18 mm		Powder	2.529	< 0.01	
B8-L7_20-23 mm		Powder	2.536	< 0.01	
B8-L8_0-3 mm		Powder	2.506	0.03	
B8-L8_3-5 mm		Powder	2.554	0.02	
B8-L8_5-8 mm		Powder	2.545	0.01	
B8-L8_10-13 mm		Powder	2.608	< 0.01	
B8-L8_15-18 mm		Powder	2.543	< 0.01	
B8-L8_20-23 mm		Powder	2.532	< 0.01	

INFO

Method
The test was performed using the potentiometric titration method of the standard SFS-EN 14629:2007, using samples provided by the customer. A sufficient amount of powdered sample was drilled from the structural specimens that may be included in the order before the initial treatment and titration. **The method is accredited.**

Results
The results are reported as weight percentages of the dry weight of the concrete sample with two decimal precision. A result labeled as *"< detection limit"* indicates a result that falls below the detection limit. These results only apply to the samples analyzed. Parts of the report should not be copied.

Storage of samples
The remaining sample materials will be stored for six months, after which they will be disposed of. If you wish to have the sample materials returned, please contact the person who signed the report.

7.3 Appendix (C) – Petrographic analysis (thin-sections) report

3012

MITTA

MACROANALYSIS – observations

Sample	B2 L7	**Ref. no**	3012
Structure	Test cube, cut	**Size**	100 mm x 100 mm x 43 mm

Observations	
Aggregate	Mostly sub-rounded, some angular granitoids, Ø < 15 mm.
Paste	Dark grey, smooth to touch.
Compaction and air voids	Moderate, voids mostly Ø < 3 mm.
Reinforcement	-
Surfaces and coatings	The top and the bottom surfaces are cut. Three of the side surfaces are coated with glossy finished gray paint. One side surface is uncoated and darkened or stained concrete.
Layers and adhesion	-
Faults and deterioration	-
Other observations	The sample surfaces are named in relation to sample ID. The top surface is above the sample ID and the bottom surface is under it.

3012

MITTA

MICROANALYSIS - observations

Sample	B2 L7	**Depth studied**	0–43 mm from the cut bottom surface
Thin section	BBA1	**Size**	28 x 43 mm

Aggregate, coarse	Mostly sub-rounded granitoids.
Aggregate, fine	Mostly subrounded to subangular and some angular quartz and feldspar grains, also granitoid and sandstone aggregates. In addition, a single chlorite rich aggregate.
Adhesion of aggregate	The adhesion of the aggregates is mostly tight.
Paste	The paste contains coarse grained Portland cement and isotropic particles, which resemble slag, but can also be mineral grains. The degree of hydration is normal to high. The microstructure is homogenous, the paste has normal to slightly low microporosity.
Carbonation	The paste is non-carbonated at the study area.
$Ca(OH)_2$	Fine- to medium-grained crystals, which are evenly distributed in the paste.
Cracking, surface	-
Cracking, inner	Quite weak, mostly unoriented microcracking, which in few cases cuts aggregates. One aggregate cutting microcrack parallel to the surface were observed at a depth of 5 mm from the cut bottom surface.
Voids	There are only a few small, rounded/spherical voids in the study area. The amount of bigger (Ø < 2,3 mm), and almost spherical or oval voids is also quite low.
Secondary deposits	Slightly low to moderate amount of ettringite and calcium hydroxide crystals in the voids. The amount of the ettringite and the $Ca(OH)_2$ is abundant near the cut bottom surface, where most of the smallest voids (Ø < 0,24 mm) have been filled.
ASR	-
Other observations	-

Figures on the next page.

3012

MITTA

MICROANALYSIS - figures

Sample	B2 L7
Thin section	BBA1

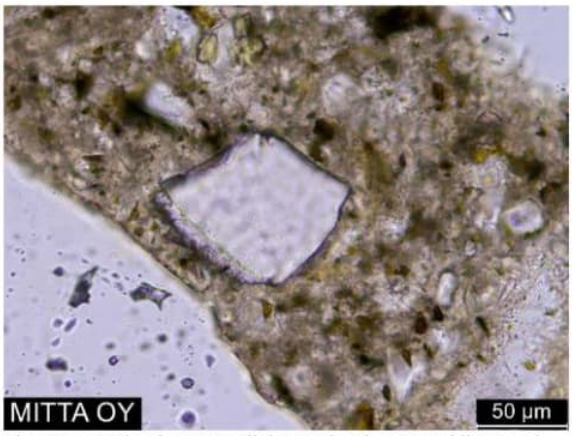

Figure 2. Portland cement clinker and a slag resembling particle in the paste. PPL

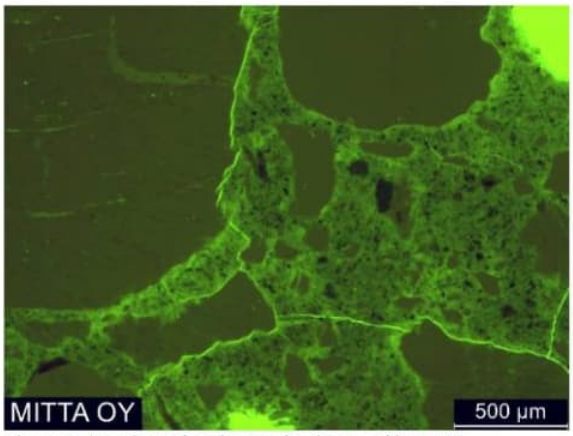

Figure 3. Unoriented, quite weak microcracking. UVL

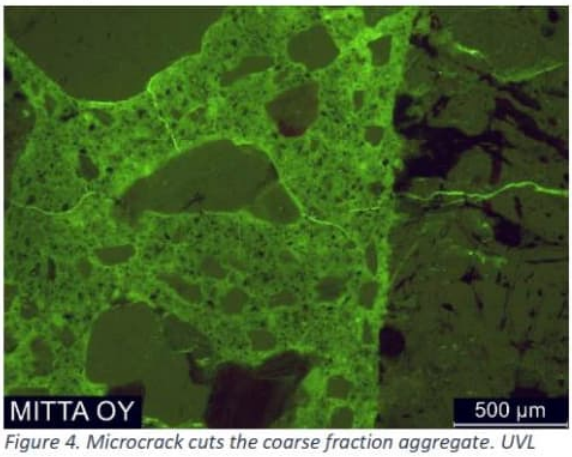

Figure 4. Microcrack cuts the coarse fraction aggregate. UVL

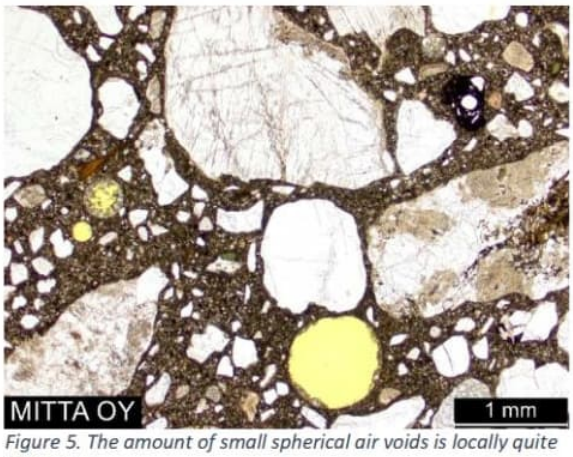

Figure 5. The amount of small spherical air voids is locally quite low. PPL

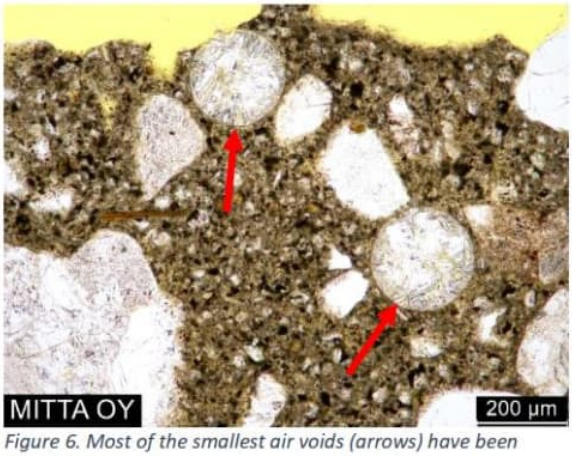

Figure 6. Most of the smallest air voids (arrows) have been filled with ettringite near the cut bottom surface. PPL

PPL = plane polarized light, UVL = ultraviolet light

3012

MITTA

MACROANALYSIS – observations

Sample	B2 L8	**Ref. no**	3012
Structure	Test cube, cut	**Size**	100 mm x 100 mm x 43 mm

Observations	
Aggregate	Mostly sub-rounded, some angular granitoids, Ø < 14 mm.
Paste	Dark grey, smooth to touch.
Compaction and air voids	Moderate, voids mostly Ø < 4 mm.
Reinforcement	-
Surfaces and coatings	The top and the bottom surfaces are cut. Three of the side surfaces are coated with glossy finished gray paint. One side surface is uncoated and darkened or stained concrete.
Layers and adhesion	-
Faults and deterioration	-
Other observations	The sample surfaces are named in relation to sample ID. The top surface is above the sample ID and the bottom surface is under it.

3012

MICROANALYSIS - observations

Sample	B2 L8	**Depth studied**	0–43 mm from the top cut surface
Thin section	BBA2	**Size**	28 x 43 mm

Aggregate, coarse	Mostly sub-rounded and rounded granitoid and amphibolite aggregates.
Aggregate, fine	Mostly subrounded to subangular and some angular quartz and feldspar grains, also granitoid and amphibolite aggregates.
Adhesion of aggregate	The adhesion of the aggregates is mostly tight.
Paste	The paste contains coarse grained Portland cement and isotropic particles, which resemble slag, but can also be mineral grains. The degree of hydration is high. The microstructure is mostly homogenous, the paste has normal to slightly low microporosity.
Carbonation	The paste is non-carbonated at the study area.
$Ca(OH)_2$	Fine- to medium-grained crystals, which are evenly distributed in the paste.
Cracking, surface	-
Cracking, inner	Quite weak, unoriented microcracking, which does not cut the aggregates.
Voids	There are only a few small, rounded/spherical voids in the study area. The amount of bigger (Ø < 3,4 mm), and almost spherical or irregular voids is also quite low.
Secondary deposits	Slightly low to moderate amount of ettringite crystals in the voids. Some of the smallest voids (Ø < 0,4 mm) have almost been filled.
ASR	-
Other observations	-

Figures on the next page.

3012

MITTA

MICROANALYSIS - figures

Sample	B2 L8
Thin section	BBA2

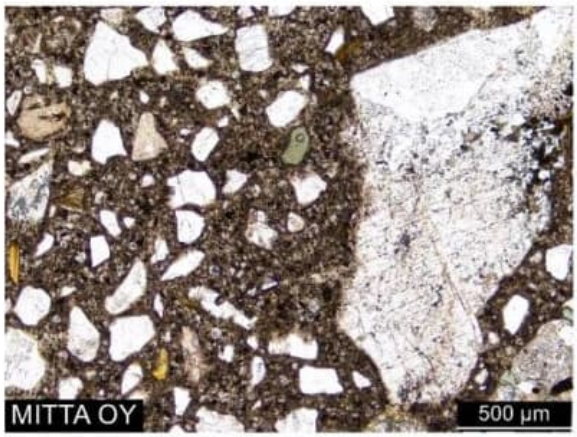

Figure 8. Microtexture of the paste is homogenous. PPL

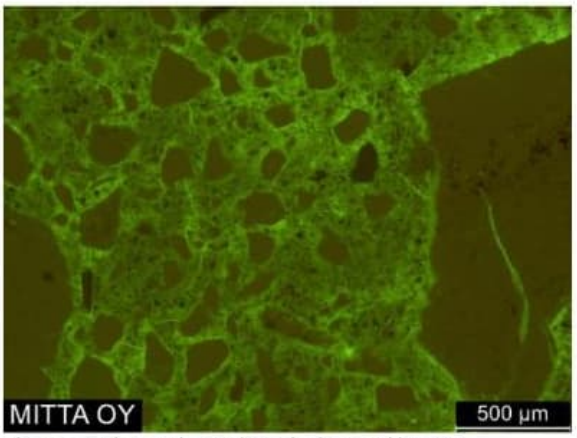

Figure 9. Quite weak, unoriented microcracking. UVL

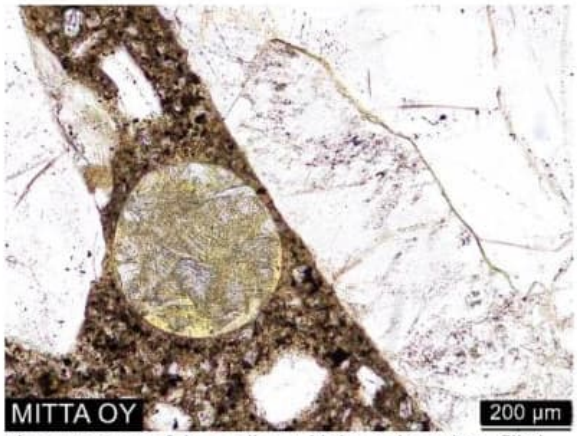

Figure 10. Some of the smallest voids have almost been filled with ettringite crystals. PPL

PPL = plane polarized light, UVL = ultraviolet light

3012

MITTA

MACROANALYSIS – observations

Sample	B2 VLJ	**Ref. no**	3012
Structure	Test cube, cut	**Size**	100 mm x 100 mm x 65 mm

Observations	
Aggregate	Mostly sub-rounded and rounded, some angular and partly angular granitoids, Ø < 12 mm.
Paste	Dark grey, smooth to touch.
Compaction and air voids	Moderate, voids mostly Ø < 4 mm.
Reinforcement	-
Surfaces and coatings	All the other surfaces are uncoated concrete, the bottom surface is cut.
Layers and adhesion	-
Faults and deterioration	-
Other observations	The sample surfaces are named in relation to sample ID. The top surface is above the sample ID and the bottom surface is under it. There is a metal bolt etc. on the top surface.

3012

MITTA

MICROANALYSIS - observations

Sample	B2 VLJ	**Depth studied**	0–47 mm from the top surface
Thin section	BBA3	**Size**	28 x 47 mm

Aggregate, coarse	Mostly sub-rounded granitoids.
Aggregate, fine	Mostly subrounded to subangular and some angular quartz and feldspar grains, also granitoid and amphibolite aggregates.
Adhesion of aggregate	The adhesion of the aggregates is mostly tight.
Paste	The paste contains coarse grained Portland cement and isotropic particles, which resemble slag, but can also be mineral grains. The degree of hydration is normal to high. The microstructure is quite homogenous, the paste has normal microporosity.
Carbonation	The paste is non-carbonated at the study area.
$Ca(OH)_2$	Medium- to coarse-grained crystals, which are quite evenly distributed in the paste.
Cracking, surface	A few microcracks open to the top surface and connect to the microcracking in inner parts at a depth of approx. 4 mm from the top surface.
Cracking, inner	Quite weak, unoriented microcracking, which does not cut the aggregates.
Voids	There are only a few small, rounded/spherical voids in the study area. The amount of bigger (Ø < 3 mm), and almost spherical or irregular voids is also quite low.
Secondary deposits	Slightly low to moderate amount of ettringite crystals in the voids. In addition, the calcium hydroxide crystals are filling most of the smallest voids (Ø < 0,4 mm).
ASR	-
Other observations	There is a < 0,16 mm thick calcite crust on the top surface.

Figures on the next page.

3012

MITTA

MICROANALYSIS - figures

Sample	B2 VLJ
Thin section	BBA3

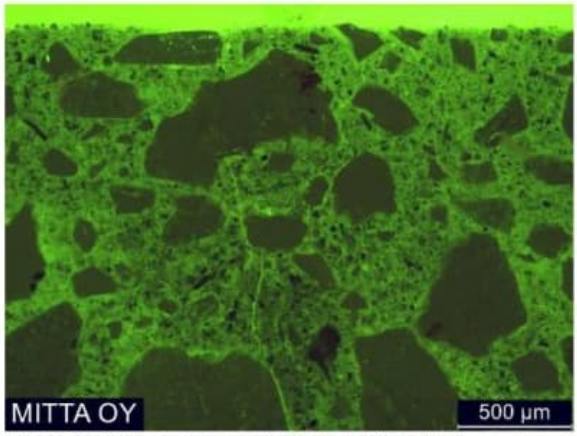

Figure 12. Microcrack opens to the top surface. UVL

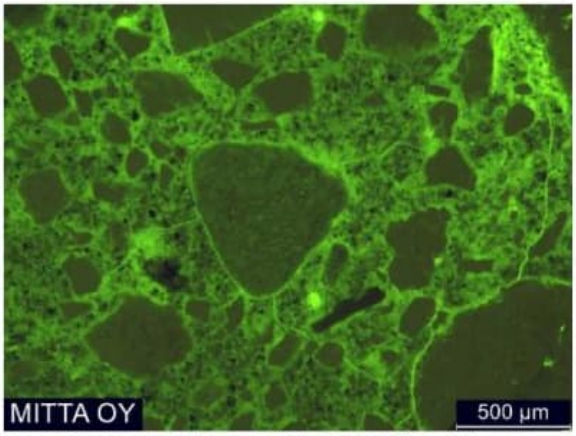

Figure 13. Quite weak, unoriented microcracking. UVL

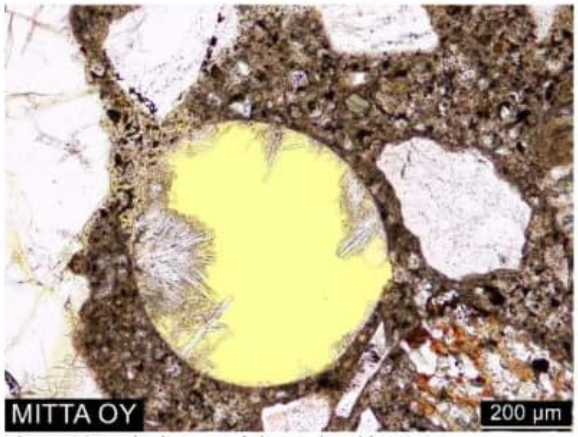

Figure 14. Ettringite crystals in an air void. PPL

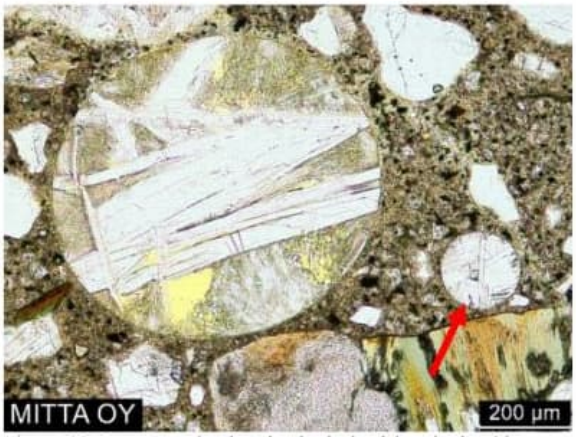

Figure 15. Coarse-grained and euhedral calcium hydroxide crystals (and ettringite) in air voids. The smaller void (arrow) is completely filled with $Ca(OH)_2$. PPL

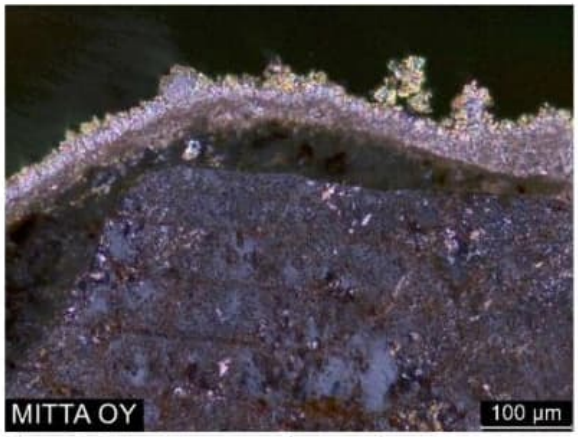

Figure 16. Thin calcite crust on the top surface. XPL

PPL = plane polarized light, XPL = cross polarized light, UVL = ultraviolet light

3012

MITTA

MACROANALYSIS – observations

Sample	B5 L7	**Ref. no**	3012
Structure	Test cube, cut	**Size**	100 mm x 100 mm x 41 mm

Observations	
Aggregate	Mostly sub-rounded, some angular granitoids, Ø < 16 mm.
Paste	Grey, smooth to touch.
Compaction and air voids	Moderate, voids mostly Ø < 4,5 mm.
Reinforcement	-
Surfaces and coatings	The top and the bottom surfaces are cut. Three of the side surfaces are coated with glossy finished gray paint. One side surface is uncoated and darkened or stained concrete.
Layers and adhesion	-
Faults and deterioration	-
Other observations	The sample surfaces are named in relation to sample ID. The top surface is above the sample ID and the bottom surface is under it.

3012

MITTA

MICROANALYSIS - observations

Sample	B5 L7	**Depth studied**	0–41 mm from the cut top surface
Thin section	BBA4	**Size**	28 x 41 mm

Aggregate, coarse	Mostly sub-rounded granitoid and gabbro aggregates.
Aggregate, fine	Mostly subrounded to subangular and some angular quartz and feldspar grains, also granitoid and gabbro aggregates.
Adhesion of aggregate	The adhesion of the aggregates is mostly tight, only a single air void was observed on the aggregate surface.
Paste	The paste contains coarse grained Portland cement, slag, silica fume, fly ash and lime filler. Silica fume occurs in lumps (Ø < 0,18 mm). The degree of hydration is normal to high. The microstructure is homogenous, the paste has slightly low microporosity.
Carbonation	The paste is uncarbonated in the study area.
$Ca(OH)_2$	Fine-grained crystals, which are evenly distributed in the paste.
Cracking, surface	-
Cracking, inner	Moderate to quite strong, unoriented microcracking, which in few cases cuts the aggregates. Two fine cracks, which do not cut the aggregates, extend to a depth of 14,5 mm from the cut top surface. The cracks are perpendicular to the surface and their maximum width is 0,015 mm.
Voids	There are only a few small, rounded/spherical voids in the study area. The amount of bigger (Ø < 3 mm), and almost spherical or oval voids is quite low.
Secondary deposits	Slightly low amount of ettringite crystals in the voids. Some of the smallest voids (Ø < 0,08 mm) have been filled with the ettringite.
ASR	-
Other observations	-

Figures on the next page.

3012

MITTA

MICROANALYSIS - figures

Sample	B5 L7
Thin section	BBA4

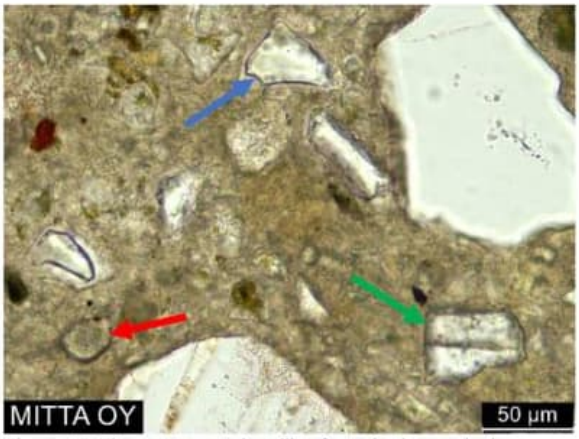

Figure 18. The paste contains silica fume (red arrow), slag (blue arrow) and limestone filler (green arrow). PPL

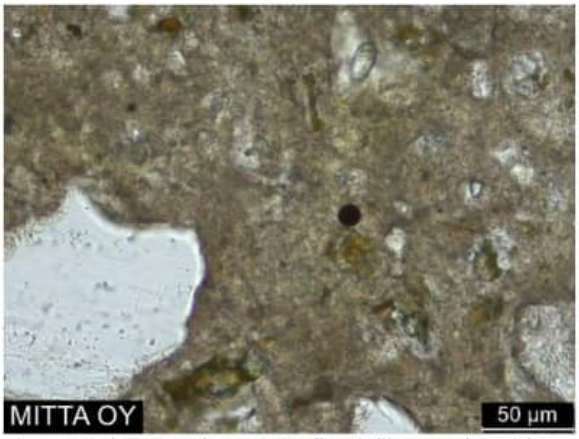

Figure 19. The paste also contains fly ash-like, round particles. PPL

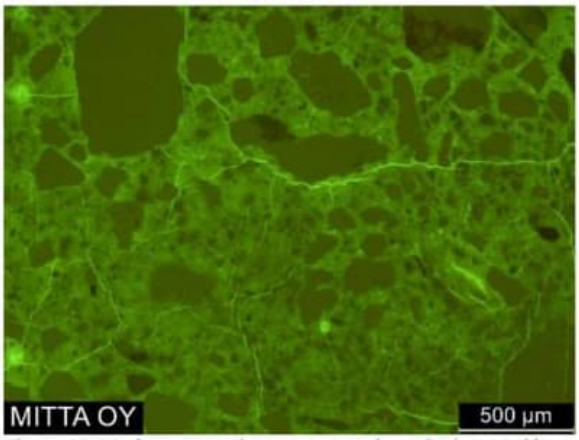

Figure 20. Moderate to quite strong, unoriented microcracking. UVL

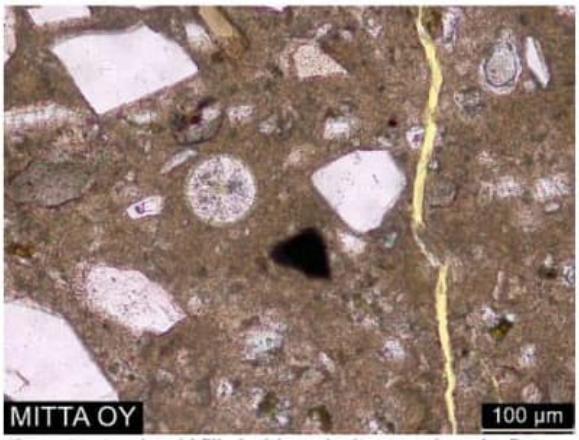

Figure 21. An air void filled with ettringite crystals and a fine crack perpendicular to the surface. PPL

PPL = plane polarized light, UVL = ultraviolet light

3012

MITTA

MACROANALYSIS – observations

Sample	B5 L8	**Ref. no**	3012
Structure	Test cube, cut	**Size**	100 mm x 100 mm x 42 mm

Observations	
Aggregate	Mostly sub-rounded, some angular granitoids, Ø < 13 mm.
Paste	Grey, smooth to touch.
Compaction and air voids	Moderate, voids mostly Ø < 4,5 mm.
Reinforcement	-
Surfaces and coatings	The top surface and three of the side surfaces are coated with glossy finished gray paint. One side surface is uncoated and darkened or stained concrete. The bottom surface is cut.
Layers and adhesion	-
Faults and deterioration	-
Other observations	The sample surfaces are named in relation to sample ID. The top surface is above the sample ID and the bottom surface is under it.

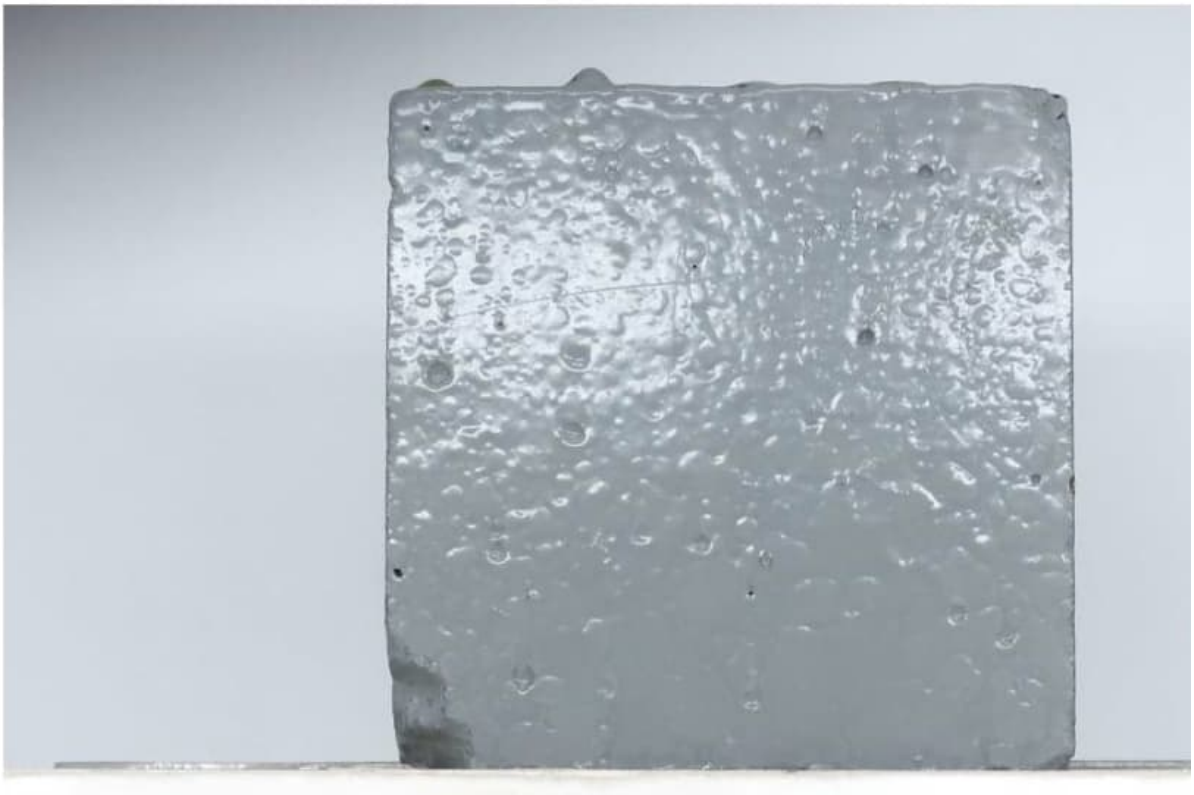

3012

MITTA

MICROANALYSIS - observations

Sample	B5 L8	**Depth studied**	0–42 mm from the top surface
Thin section	BBA5	**Size**	28 x 42 mm

Aggregate, coarse	Mostly sub-rounded granitoids.
Aggregate, fine	Mostly subrounded to subangular and some angular quartz and feldspar grains, also granitoid and sandstone aggregates. In addition, a single gabbro aggregate.
Adhesion of aggregate	The adhesion of the aggregates is mostly tight, only a single air void was observed on the aggregate surface.
Paste	The paste contains coarse grained Portland cement, slag, silica fume, fly ash and lime filler. Silica fume occurs in quite large (Ø < 0,3 mm) lumps. The degree of hydration is normal to high. The microstructure is homogenous, the paste has slightly low microporosity.
Carbonation	On average 1 mm, maximum at a depth of 9,5 mm from the top surface following the microcracks. Carbonation reaches approx. 0,5 mm away from the crack edges.
$Ca(OH)_2$	Fine-grained crystals, which are evenly distributed in the paste.
Cracking, surface	A few microcracks open to the top surface and connect to the microcracking in inner parts at a depth of approx. 5 mm from the top surface.
Cracking, inner	Quite strong, unoriented microcracking, which in few cases cuts the aggregates.
Voids	There are only a few small, rounded/spherical voids in the study area. The amount of bigger (Ø < 2 mm), and almost spherical or oval voids is low.
Secondary deposits	Slightly low to moderate amount of ettringite crystals in the voids. Some of the smallest voids (Ø < 0,15 mm) have almost been filled with the ettringite.
ASR	The largest silica fume lumps have cracked and, in some cases the microcracking continues to the paste not further than 2 mm from the lump.
Other observations	There is a < 0,15 mm thick coating on the top surface. The coating has two layers. The upper layer is almost black and opaque (PPL), and it has very small fiber and/or plate like particles. The lower layer is isotropic and white (PPL). The coating is detached from the concrete. There is a very thin calcite crust under the coating and on the concrete surface.

Figures on the next page.

3012

MITTA

MICROANALYSIS - figures

Sample	B5 L8
Thin section	BBA5

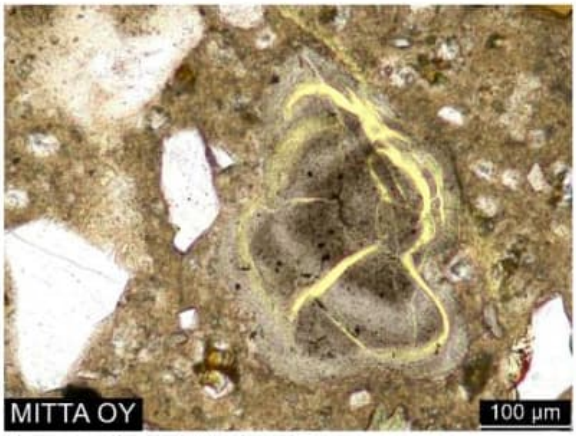

Figure 23. A lump of silica fume. PPL

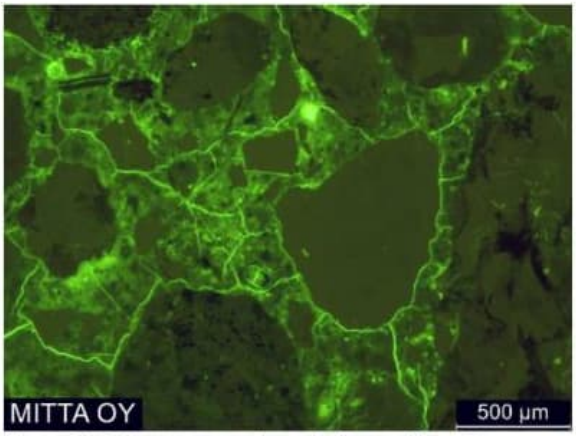

Figure 24. Quite strong, unoriented microcracking. UVL

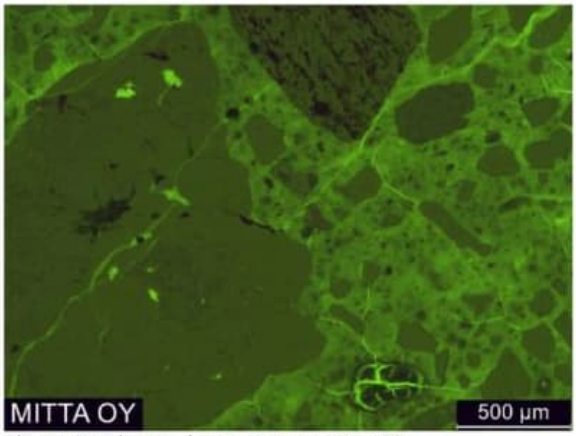

Figure 25. Microcrack cuts an aggregate. UVL

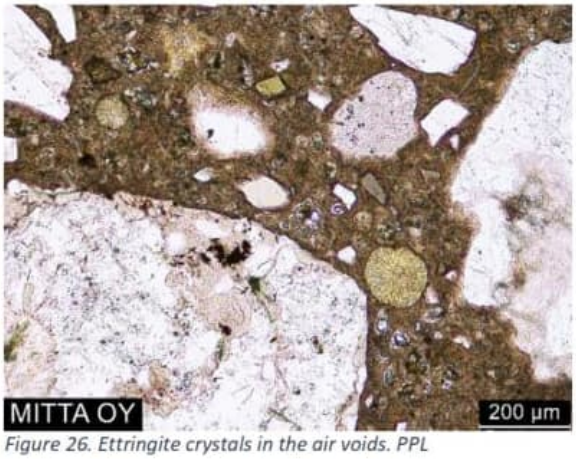

Figure 26. Ettringite crystals in the air voids. PPL

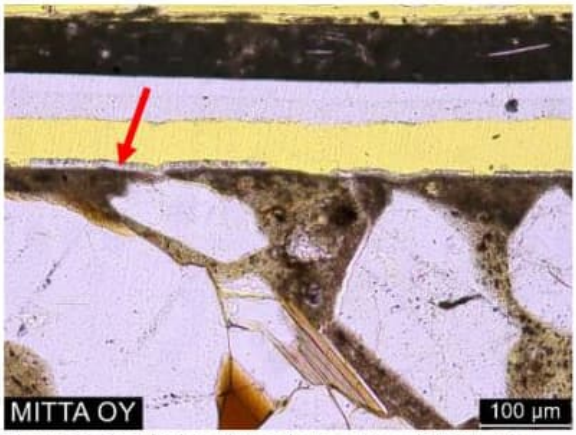

Figure 27. Detached coating and a very thin calcite crust (arrow) on the top surface of the sample. PPL

PPL = plane polarized light, UVL = ultraviolet light

3012

MITTA

MACROANALYSIS – observations

Sample	B5 VLJ	**Ref. no**	3012
Structure	Test cube, cut	**Size**	100 mm x 100 mm x 45 mm

Observations	
Aggregate	Mostly sub-rounded, some angular granitoids, Ø < 15 mm.
Paste	Grey, smooth to touch.
Compaction and air voids	Moderate, voids mostly Ø < 6,5 mm.
Reinforcement	-
Surfaces and coatings	The top and the bottom surfaces are cut. The side surfaces are uncoated concrete.
Layers and adhesion	-
Faults and deterioration	-
Other observations	The sample surfaces are named in relation to sample ID. The top surface is above the sample ID and the bottom surface is under it.

3012

MITTA

MICROANALYSIS - observations

Sample	B5 VLJ	**Depth studied**	0–45 mm from the cut bottom surface
Thin section	BBA6	**Size**	28 x 45 mm

Aggregate, coarse	Mostly angular, some sub-rounded granitoids. In addition, a single rounded granitoid aggregate and a single garnet-rich altered aggregate.
Aggregate, fine	Mostly subrounded to subangular and some angular quartz and feldspar grains, also granitoid aggregates.
Adhesion of aggregate	The adhesion of the aggregates is mostly tight, only a couple air voids were observed on the aggregate surface.
Paste	The paste contains coarse grained Portland cement, slag, silica fume, fly ash and lime filler. Silica fume occurs in quite large (Ø < 0,25 mm) lumps. The degree of hydration is normal to high. The microstructure is homogenous, the paste has slightly low microporosity.
Carbonation	The paste is uncarbonated in the study area.
$Ca(OH)_2$	Fine-grained crystals, which are evenly distributed in the paste.
Cracking, surface	-
Cracking, inner	Quite strong, unoriented microcracking, which in few cases cuts the aggregates.
Voids	The amount of small, rounded/spherical voids is minor to moderate in the study area. The amount of bigger (Ø < 2,4 mm), and almost spherical or oval voids is quite low.
Secondary deposits	Slightly low to moderate amount of ettringite crystals in the voids. Most of the smallest voids (Ø < 0,12 mm) have been filled with the ettringite.
ASR	The largest silica fume lumps have cracked and, in some cases the microcracking continues to the paste not further than 0,5 mm from the lump.
Other observations	-

Figures on the next page.

3012

MITTA

MICROANALYSIS - figures

Sample	B5 VLJ
Thin section	BBA6

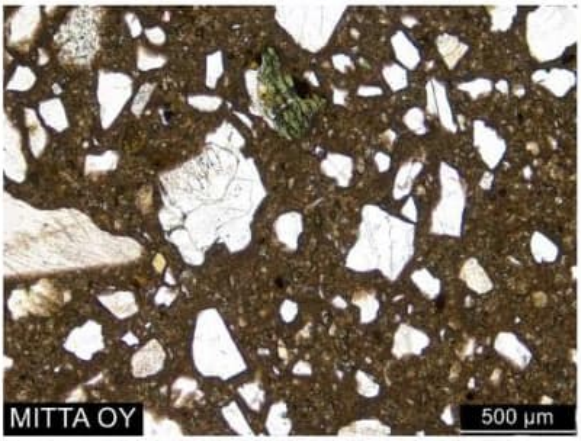

Figure 29. Adhesion of the aggregates is mostly tight. PPL

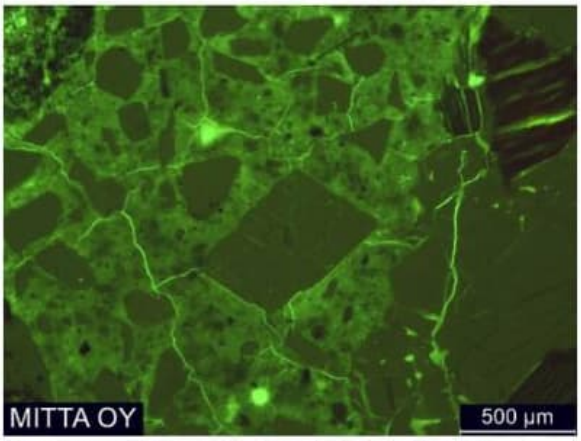

Figure 30. Quite strong, unoriented microcracking. UVL

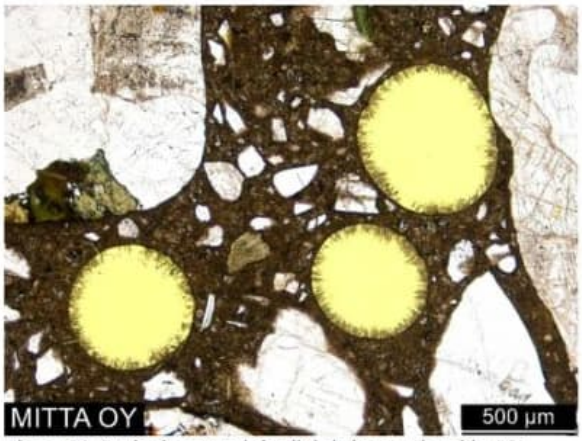

Figure 31. Ettringite crystals in slightly larger air voids. PPL

Figure 32. Cracking has proceeded to the paste from the silica fume lump. PPL

PPL = plane polarized light, UVL = ultraviolet light

3012

MITTA

MACROANALYSIS – observations

Sample	B8 L7	**Ref. no**	3012
Structure	Test cube, cut	**Size**	100 mm x 100 mm x 50 mm

Observations	
Aggregate	Mostly sub-rounded, some angular granitoids, Ø < 15 mm.
Paste	Greenish grey, smooth to touch.
Compaction and air voids	Moderate, voids mostly Ø < 6,5 mm.
Reinforcement	-
Surfaces and coatings	The top and the bottom surfaces are cut. Three of the side surfaces are coated with glossy finished gray paint. One side surface is uncoated and darkened or stained concrete.
Layers and adhesion	-
Faults and deterioration	-
Other observations	The sample surfaces are named in relation to sample ID. The top surface is above the sample ID and the bottom surface is under it.

3012

MITTA

MICROANALYSIS - observations

Sample	B8 L7	**Depth studied**	0–47 mm from the cut top surface
Thin section	BBA7	**Size**	28 x 47 mm

Aggregate, coarse	Mostly sub-rounded and rounded, some angular granitoid, amphibolite and gabbro aggregates.
Aggregate, fine	Mostly subrounded to subangular and some angular quartz and feldspar grains, also granitoid and a single sandstone and amphibolite aggregates.
Adhesion of aggregate	The adhesion of the aggregates is mostly tight, a few short < 0,02 mm wide cracks were observed on the aggregate surface.
Paste	The paste contains coarse grained Portland cement, lime filler, abundantly slag and small opaque particles. The degree of hydration is normal to high. The paste is rather opaque due to large amount of slag, and it has a strong greenish tint. The microstructure is mostly homogenous, and the paste mostly has a very low microporosity. However, in some cases the areas surrounding the aggregate appear to have higher microporosity.
Carbonation	The paste is uncarbonated in the study area.
$Ca(OH)_2$	The paste appears depleted from calcium hydroxide.
Cracking, surface	-
Cracking, inner	Quite strong, unoriented microcracking, which in few cases cuts the aggregates.
Voids	There are only a few small, rounded/spherical voids in the study area. The amount of bigger (Ø < 3,5 mm), and almost spherical or oval voids is moderate.
Secondary deposits	-
ASR	-
Other observations	-

Figures on the next page.

3012

MITTA

MICROANALYSIS - figures

Sample	B8 L7
Thin section	BBA7

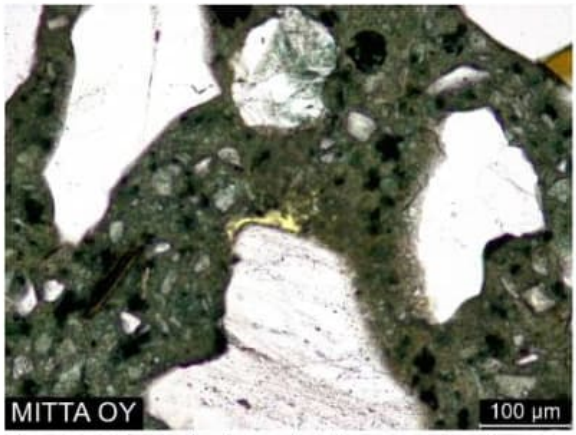

Figure 34. A short adhesion crack on the aggregate surface. PPL

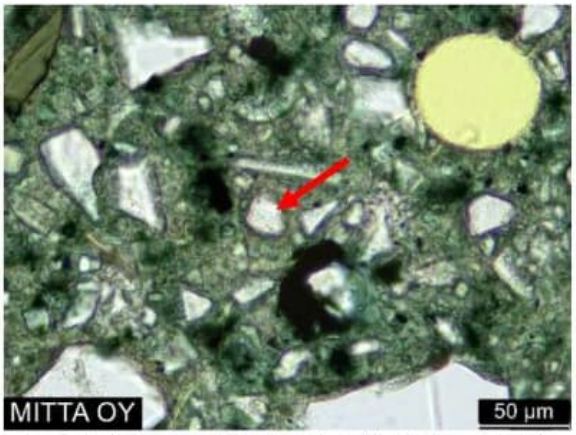

Figure 35. The paste contains limestone filler (red arrow) and abundantly slag particles (white and angular). PPL

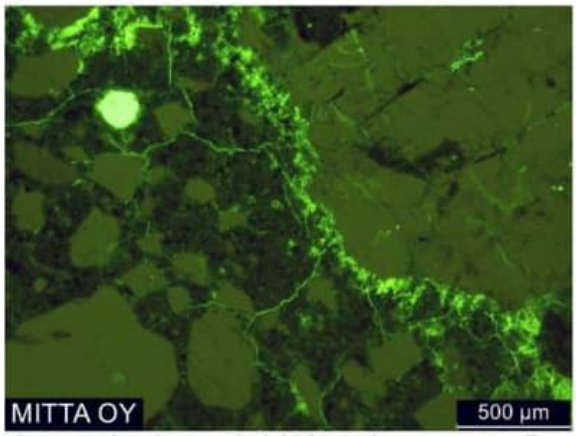

Figure 36. The microporosity is higher in the areas surrounding some of the aggregates. UVL

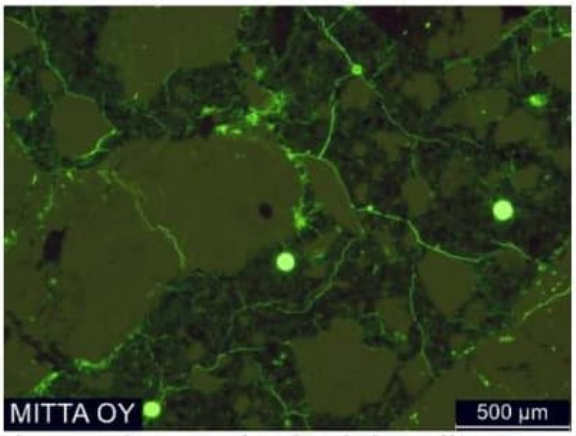

Figure 37. Quite strong and unoriented microcracking. UVL

PPL = plane polarized light, UVL = ultraviolet light

3012

MITTA

MACROANALYSIS – observations

Sample	B8 L8	**Ref. no**	3012
Structure	Test cube, cut	**Size**	100 mm x 100 mm x 53 mm

Observations	
Aggregate	Mostly sub-rounded, some angular granitoids, Ø < 12 mm.
Paste	Greenish grey, smooth to touch.
Compaction and air voids	Moderate, voids mostly Ø < 4,5 mm.
Reinforcement	-
Surfaces and coatings	The top surface and three of the side surfaces are coated with glossy finished gray paint. One side surface is uncoated concrete. The bottom surface is cut.
Layers and adhesion	-
Faults and deterioration	-
Other observations	The sample surfaces are named in relation to sample ID. The top surface is above the sample ID and the bottom surface is under it.

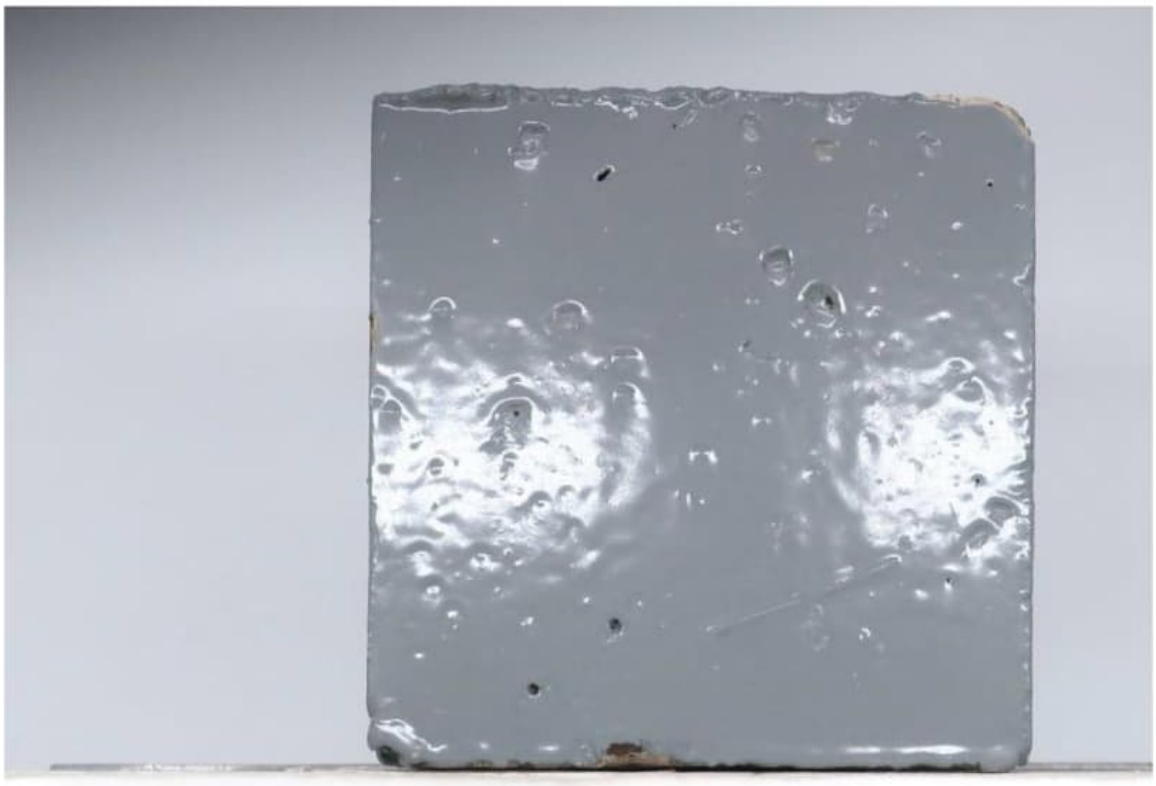

3012

MITTA

MICROANALYSIS - observations

Sample	B8 L8	**Depth studied**	0–47 mm from the cut top surface
Thin section	BBA8	**Size**	28 x 47 mm

Aggregate, coarse	Mostly sub-rounded and rounded, some angular granitoid and gabbro aggregates.
Aggregate, fine	Mostly subrounded to subangular and some angular quartz and feldspar grains, also granitoid and a couple of amphibolite aggregates.
Adhesion of aggregate	The adhesion of the aggregates is mostly tight, a couple air voids were observed on the aggregate surface.
Paste	The paste contains coarse grained Portland cement, lime filler, abundantly slag and small opaque particles. The degree of hydration is normal to high. The paste is rather opaque due to large amount of slag, and it has a strong greenish tint. The microstructure is mostly homogenous, and the paste mostly has a very low microporosity. However, in some cases the areas surrounding the aggregate appear to have higher microporosity.
Carbonation	On average 5,5 mm, maximum at a depth of 8 mm from the cut top surface.
$Ca(OH)_2$	The paste appears depleted from calcium hydroxide.
Cracking, surface	-
Cracking, inner	Quite strong, unoriented microcracking, which in few cases cuts the aggregates.
Voids	There are only a few small, rounded/spherical voids in the study area. The amount of bigger (Ø < 2,7 mm), and almost spherical or oval voids is moderate.
Secondary deposits	-
ASR	-
Other observations	-

Figures on the next page.

3012

MITTA

MICROANALYSIS - figures

Sample	B8 L8
Thin section	BBA8

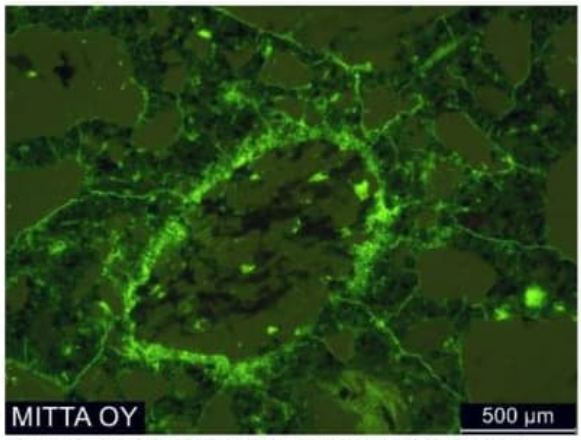

Figure 39. A more microporous area surrounding an aggregate. UVL

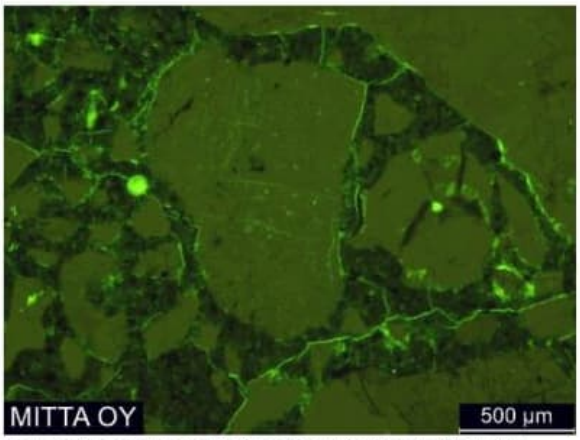

Figure 40. Quite strong and unoriented microcracking. UVL

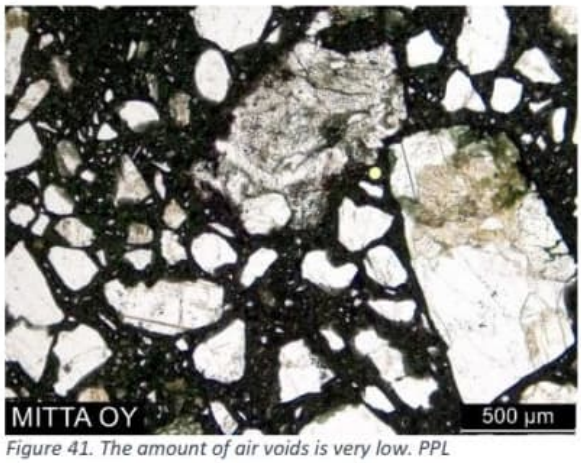

Figure 41. The amount of air voids is very low. PPL

PPL = plane polarized light, UVL = ultraviolet light

3012

MITTA

MACROANALYSIS – observations

Sample	B8 VLJ	**Ref. no**	3012
Structure	Test cube, cut	**Size**	97 mm x 97 mm x 33 mm

Observations	
Aggregate	Mostly sub-rounded, some angular granitoids, Ø < 16 mm.
Paste	Greenish grey, smooth to touch.
Compaction and air voids	Moderate, voids mostly Ø < 5 mm.
Reinforcement	-
Surfaces and coatings	All the other surfaces are cut, but two side surfaces are uncoated concrete.
Layers and adhesion	-
Faults and deterioration	-
Other observations	The sample surfaces are named in relation to sample ID. The top surface is above the sample ID and the bottom surface is under it.

3012

MITTA

MICROANALYSIS - observations

Sample	B8 VLJ	**Depth studied**	0–33 mm from the cut top surface
Thin section	BBA9	**Size**	28 x 33 mm

Aggregate, coarse	Mostly sub-rounded granitoid and gabbro aggregates.
Aggregate, fine	Mostly subrounded to subangular and some angular quartz and feldspar grains, also granitoid and a couple of amphibolite or gabbro aggregates.
Adhesion of aggregate	The adhesion of the aggregates is mostly tight.
Paste	The paste contains coarse grained Portland cement, lime filler, silica fume, abundantly slag and small opaque particles. The silica fume occurs mostly in quite small (Ø < 0,1 mm) lumps. A single Ø 0,2 mm was observed. The degree of hydration is normal to high. The paste is rather opaque due to large amount of slag, and it has a strong greenish tint. The microstructure is mostly homogenous, and the paste mostly has a very low microporosity. However, in some cases the areas surrounding the aggregate appear to have higher microporosity.
Carbonation	The paste is uncarbonated in the study area.
$Ca(OH)_2$	The paste appears depleted from calcium hydroxide.
Cracking, surface	-
Cracking, inner	Quite strong, unoriented microcracking, which in few cases cuts the aggregates.
Voids	There are only a few small, rounded/spherical voids in the study area. The amount of bigger (Ø < 1,8 mm), and almost spherical or oval voids is low.
Secondary deposits	-
ASR	-
Other observations	-

Figures on the next page.

3012

MITTA

MICROANALYSIS - figures

Sample	B8 VLJ
Thin section	BBA9

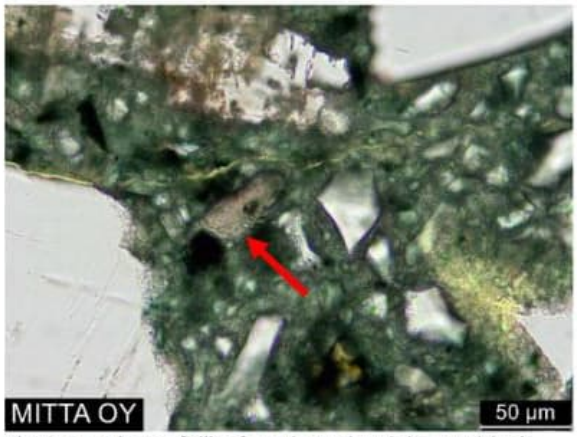

Figure 43. A lump of silica fume (arrow) and slag particles in the paste. PPL

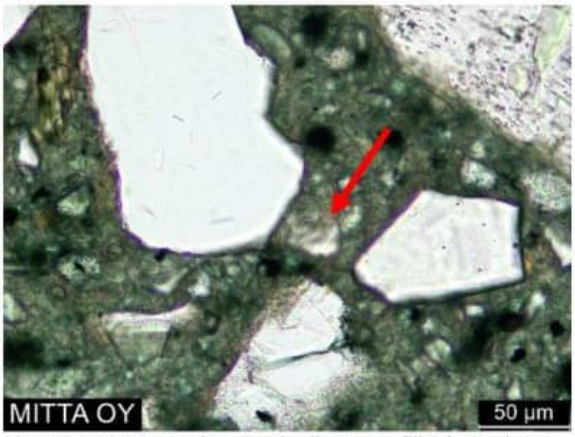

Figure 44. The paste also contains limestone filler (arrow). PPL

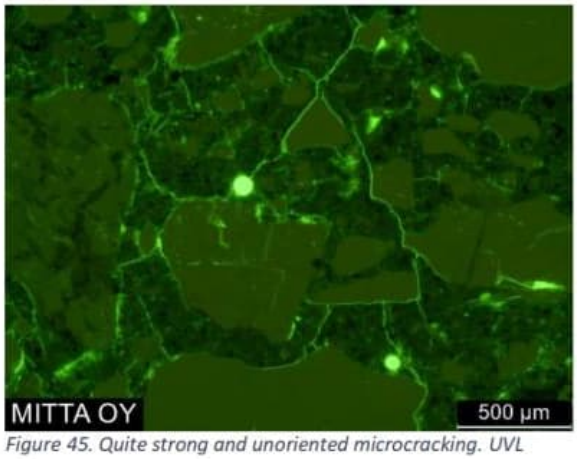

Figure 45. Quite strong and unoriented microcracking. UVL

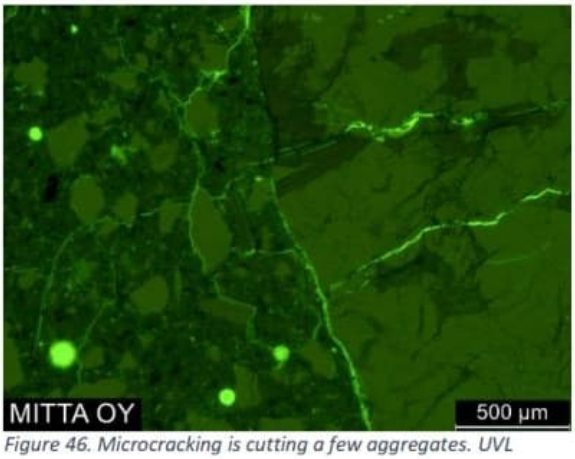

Figure 46. Microcracking is cutting a few aggregates. UVL

PPL = plane polarized light, UVL = ultraviolet light